

# A phosphoinositide 5-phosphatase from *Solanum tuberosum* is activated by PAMP-treatment and may antagonize phosphatidylinositol 4,5-bisphosphate at *Phytophthora infestans* infection sites

Juliane Rausche<sup>1</sup>, Irene Stenzel<sup>2</sup>, Ron Stauder<sup>1</sup>, Marta Fratini<sup>2</sup> , Marco Trujillo<sup>3</sup> , Ingo Heilmann<sup>2</sup>  and Sabine Rosahl<sup>1</sup> 

<sup>1</sup>Department of Stress and Developmental Biology, Leibniz Institute of Plant Biochemistry, Weinberg 3, Halle (Saale) D-06120, Germany; <sup>2</sup>Department of Cellular Biochemistry, Institute of Biochemistry and Biotechnology, Martin Luther University Halle-Wittenberg, Kurt Mothes-Str. 3, Halle (Saale) D-06120, Germany; <sup>3</sup>Independent Research Group Protein Ubiquitylation, Leibniz Institute of Plant Biochemistry, Weinberg 3, Halle (Saale) D-06120, Germany

Author for correspondence:

Ingo Heilmann

Email: [ingo.heilmann@biochemtech.uni-halle.de](mailto:ingo.heilmann@biochemtech.uni-halle.de)

Received: 6 September 2018

Accepted: 27 July 2020

New Phytologist (2021) 229: 469–487

doi: 10.1111/nph.16853

**Key words:** Pep-13, *Phytophthora infestans*, potato, protein stability.

## Summary

- Potato (*Solanum tuberosum*) plants susceptible to late blight disease caused by the oomycete *Phytophthora infestans* display enhanced resistance upon infiltration with the pathogen-associated molecular pattern (PAMP), Pep-13. Here, we characterize a potato gene similar to Arabidopsis 5-phosphatases which was identified in transcript arrays performed to identify Pep-13 regulated genes, and termed StIPP.
- Recombinant StIPP protein specifically dephosphorylated the D5-position of phosphatidylinositol 4,5-bisphosphate (PtdIns(4,5)P<sub>2</sub>) *in vitro*. Other phosphoinositides or soluble inositolpolyphosphates were not converted.
- When transiently expressed in tobacco (*Nicotiana tabacum*) pollen tubes, a StIPP-YFP fusion localized to the subapical plasma membrane and antagonized PtdIns(4,5)P<sub>2</sub>-dependent effects on cell morphology, indicating *in vivo* functionality. *Phytophthora infestans*-infection of *N. benthamiana* leaf epidermis cells resulted in relocalization of StIPP-GFP from the plasma membrane to the extra-haustorial membrane (EHM). Colocalization with the effector protein RFP-AvrB1b2 at infection sites is consistent with a role of StIPP in the plant–oomycete interaction. Correlation analysis of fluorescence distributions of StIPP-GFP and biosensors for PtdIns(4,5)P<sub>2</sub> or phosphatidylinositol 4-phosphate (PtdIns4P) indicate StIPP activity predominantly at the EHM.
- In Arabidopsis protoplasts, expression of StIPP resulted in the stabilization of the PAMP receptor, FLAGELLIN-SENSITIVE 2, indicating that StIPP may act as a PAMP-induced and localized antagonist of PtdIns(4,5)P<sub>2</sub>-dependent processes during plant immunity.

## Introduction

The hemibiotrophic oomycete *Phytophthora infestans* is the causal agent of late blight, the most devastating potato (*Solanum tuberosum*) disease worldwide. Attempts to generate resistant potato plants have previously concentrated on introducing resistance genes from wild species into cultivated potato (Fry, 2008). In addition, enhanced resistance can be induced in susceptible plants by treatment with chemicals such as β-amino butyric acid (BABA) (Cohen, 2002) or with the pathogen-associated molecular pattern (PAMP), Pep-13 (Brunner *et al.*, 2002; Halim *et al.*, 2004). The establishment of both types of resistance is dependent on salicylic acid (SA), as transgenic potato plants unable to accumulate SA fail to mount the induced resistance response (Halim

*et al.*, 2009; Eschen-Lippold *et al.*, 2010). Pep-13-activated defense responses, moreover, require jasmonic acid (Halim *et al.*, 2009).

The oligopeptide Pep-13 originates from an extracellular transglutaminase from *Phytophthora* species, and as a PAMP activates a multicomponent immune response (Brunner *et al.*, 2002). Infiltration of potato leaves with Pep-13 leads to the accumulation of SA and jasmonic acid, the activation of defense genes and to hypersensitive cell death (Halim *et al.*, 2009). An inactive analog of Pep-13, the peptide W2A, does not induce these responses (Brunner *et al.*, 2002). To elucidate the downstream mechanisms of Pep-13-mediated resistance, we have previously identified Pep-13-activated genes by microarray analyses (Landgraf *et al.*, 2014). Functional characterization of selected

candidate genes revealed a contribution of vesicle trafficking processes to the defense against *P. infestans* (Eschen-Lippold *et al.*, 2012), consistent with earlier work from the Arabidopsis model (Collins *et al.*, 2003). Based on data from Arabidopsis, the interplay of secretory and endosomal pathways contributes to controlling the abundance of immune receptors at the plasma membrane (Ben Khaled *et al.*, 2015), as receptors are actively internalized upon activation and degraded (Robatzek *et al.*, 2006). At the same time, activation of the immune response induces the secretory pathway and the delivery of receptors to the plasma membrane (Saeed *et al.*, 2019; Wang *et al.*, 2020). Vesicle trafficking is also important for the secretion of antimicrobial compounds and of callose (Schulze-Lefert, 2004; Lipka *et al.*, 2007), and transgenic potato plants with reduced expression of SYNTAXIN-RELATED 1 (SYR1) display altered membrane trafficking and altered defense responses in response to penetration by *P. infestans* (Eschen-Lippold *et al.*, 2012).

Membrane trafficking is controlled in all eukaryotes by phosphoinositides, a class of membrane lipids derived from phosphatidylinositol (PtdIns) (Thole & Nielsen, 2008; Heilmann, 2016; Gerth *et al.*, 2017b). PtdIns-monophosphates and -bisphosphates, such as phosphatidylinositol 4-phosphate (PtdIns4P) or phosphatidylinositol 4,5-bisphosphate (PtdIns(4,5)P<sub>2</sub>), can mark areas of the cytosolic face of membranes to recruit proteins, which mediate localized membrane-based processes around the sites of phosphoinositide accumulation (Thole & Nielsen, 2008; Heilmann, 2016; Gerth *et al.*, 2017b). Over the past decade, key roles in membrane trafficking have been attributed to PtdIns(4,5)P<sub>2</sub>, which is essential for polar tip growth of root hairs (Vincent *et al.*, 2005; Kusano *et al.*, 2008; Stenzel *et al.*, 2008) or pollen tubes (Ischebeck *et al.*, 2008; Sousa *et al.*, 2008; Zhao *et al.*, 2010; Hempel *et al.*, 2017), as well as for the polarization of auxin efflux carriers of the PIN-FORMED (PIN)-family in Arabidopsis (Mei *et al.*, 2012; Ischebeck *et al.*, 2013; Tejos *et al.*, 2014).

Several previous studies link phosphoinositides to plant responses to biotic stress. Suppressed accumulation of the soluble second messenger inositol 1,4,5-trisphosphate in transgenic *Arabidopsis thaliana* plants results in a changed Ca<sup>2+</sup> signature and in altered susceptibility against the pathogenic bacterium *Pseudomonas syringae* DC3000 (Hung *et al.*, 2014). A role for phosphoinositides in plant pathogen defense was recently proposed based on the observation that a fluorescent reporter for PtdIns(4,5)P<sub>2</sub> as well as a PI4P 5-kinase mediating the biosynthesis of PtdIns(4,5)P<sub>2</sub> accumulated in extra-invasive hyphal membranes upon infection of *Arabidopsis thaliana* with the pathogenic fungus *Colletotrichum higginsianum* (Shimada *et al.*, 2019). Moreover, Qin *et al.* (2020) recently identified PtdIns(4,5)P<sub>2</sub> as a susceptibility factor associating with the EHM after powdery mildew infection of Arabidopsis.

A pathogen-induced localized change in membrane phosphoinositide composition may influence the lifetime and abundance of plasma membrane proteins, which may benefit either plant or microbe. Regulation of membrane trafficking by phosphoinositides will also pertain to defense-related membrane proteins and receptors for PAMPs, such as FLAGELLIN-SENSITIVE 2

(FLS2), which are inserted into their target membranes by secretion and are recycled by endocytosis, ending their plasma membrane lifetime (Robatzek *et al.*, 2006; Wang *et al.*, 2020). A number of plasma membrane proteins, such as the NADPH-oxidase RbohD, are activated upon PAMP perception (Aibara & Miwa, 2014; Kadota *et al.*, 2014), and it might weaken an acute defense response to recycle these activated proteins at a constant rate. We hypothesized that modulation of phosphoinositides and membrane trafficking during responses to pathogen attack would contribute to the transient stabilization of activated defense proteins at the cell surface. In support of this notion, we recently demonstrated that the inhibition of the PI4P 5-kinase PIP5K6 upon perception of the bacterial PAMP flg22 results in reduced endocytosis of the NADPH-oxidase RbohD and other cargoes, correlating with increased production of reactive oxygen species in Arabidopsis (Menzel *et al.*, 2019).

In our efforts to elucidate the role of vesicle trafficking in pathogen defense in potato, we identified a Pep-13-activated gene, which we predicted to encode an inositolpolyphosphate phosphatase (IPP) and termed StIPP. In *Arabidopsis thaliana*, IPPs are represented as several large gene families, including 5-phosphatases (5-PTases) (Gillaspay, 2013; Gerth *et al.*, 2017b) and SUPPRESSOR OF ACTIN (SAC) phosphatases (Gillaspay, 2013; Gerth *et al.*, 2017b). Previously characterized IPPs display phosphatase activities against inositol-containing compounds, such as phosphoinositides or inositol polyphosphates, and are often promiscuous with regard to their accepted substrates (Gillaspay, 2013; Gerth *et al.*, 2017b). While an influence of IPPs on Arabidopsis development has previously been reported (Berdy *et al.*, 2001; Ercetin & Gillaspay, 2004; Gunesequera *et al.*, 2007; Ercetin *et al.*, 2008; Golani *et al.*, 2013), it has remained largely unclear which relevant inositol-containing metabolites were the primary reason for these effects.

Here, we provide a detailed characterization of StIPP function. Our biochemical *in vitro* studies reveal an unusually specific preference of recombinant StIPP for dephosphorylating the D5-position of PtdIns(4,5)P<sub>2</sub>, a phosphoinositide with well-characterized roles in plant membrane trafficking. The subsequent cell biological analyses support *in vivo* functionality of StIPP in plant cells and specifically at *P. infestans* infection sites, likely serving as an antagonist of PtdIns(4,5)P<sub>2</sub>-dependent processes that are part of the interaction of the host plant with the oomycete.

## Materials and Methods

### cDNA constructs

The full length coding sequence of *StIPP* (Sotub04g033080.1.1) was cloned as described previously (Eschen-Lippold *et al.*, 2010) using the primers 5'-CACCATGGAGGGACTATGTGTAAAGC-3' and 5'-GGAATATGAATACCAATTATTTGTTC-3'. The amplicon was cloned successively into pENTR™/D-TOPO® and pCR™8/GW/TOPO® (Thermo Fisher Scientific, Dreieich, Germany) and by LR recombination into pDEST-N112 (Dyson *et al.*, 2004). The resulting vector pDEST-N112-

StIPP was used for bacterial expression as N-terminal His<sub>(10)</sub>-MBP fusion. For transient expression of a StIPP-GFP fusion protein in plants, the StIPP coding region without the stop codon was amplified with Dream Taq polymerase (Thermo Fisher Scientific) using the primers 5'-ATGGAGGGACTATGTGTAAAGC-3' and 5'-TTTGTTCATTTTAAGCATAGATG-3' and cloned into pCR<sup>TM</sup>8/GW/TOPO<sup>®</sup> (Thermo Fisher Scientific) and subsequently into the binary vector pB7FWG2 by LR recombination (Karimi *et al.*, 2002). mCherry, mCherry<sub>PLC-PH</sub> and mCherry<sub>PLC-PH</sub> were amplified from plasmids and cloned into pCR<sup>TM</sup>8/GW/TOPO<sup>TM</sup> and subsequently into pGWB14 (Nakagawa *et al.*, 2007) by LR recombination. The plasmids AtPIP5K5-YFP-pLatGW, AtPIP5K5-CFP-pLatGW and YFP-pLatGW were cloned as previously described (Ischebeck *et al.*, 2008). The plasmids pLat52::mcherry-pEntry, pLat52::StIPP-YFP-pEntry, pLat52::AtPase11-YFP-pEntry and pLat52::AtSac9-mcherry-pEntry are based on the plasmid pEntryA, as previously described (Gerth *et al.*, 2017a). The Lat52 promoter sequence was amplified with SfiIA and SfiIB overhangs from the vector pLatGW (Ischebeck *et al.*, 2008) and inserted directionally into the SfiI sites of the pEntryA vector, yielding plasmid pLat52::pEntryA. The *StIPP-YFP* sequence was amplified from the vector pB7FWG2\_StIPP\_oS with the primer combination 5'-TGCATCGGCGCGCCATGGAGGGACTATGTGTAAAGCTTTTTG-3'/5'-TGCATCGGATCCTTACTTGTACAGCTCGTCCATGCCGAG-3' and cloned as a AscI/BamHI fragment into pLat52::pentryA, creating plasmid pLat52::StIPP-YFP-pEntry. The cDNA sequence for AtPase11 was amplified from Arabidopsis leaf cDNA with the primer combination 5'-TGCATCGGCGCGCCATGCCGACAATGGGGAATAAG-3'/5'-TGCATCCTCGAGACTGTTGACCCACTTCAAGCAAAG-3' and cloned as an AscI/XhoI fragment into pLat52::pentryA, yielding pLat52::AtPase11-pEntry. The coding sequence for YFP was amplified from the plasmid YFP-pLatGW (Ischebeck *et al.*, 2008) and moved as a XhoI/NotI fragment into pLat52::AtPase11-pEntry, creating the plasmid pLat52::AtPase11-YFP-pEntry. The cDNA sequence encoding AtSac9 was amplified from Arabidopsis leaf cDNA with the primer combination 5'-GATCGTCGACATGGATCTGCATCCACCAGGTG-3'/5'-GATCGCTAGCGACACTTGAAAGGCTAGTCCATTG-3' and moved as a Sall/NheI fragment into pLat52::pentryA, resulting in pLat52::AtSac9-pEntry. For the AtSac9-mCherry fusion, the mCherry sequence was amplified and moved as a NheI/NotI fragment into the vector pLat52::AtSac9-pEntry, creating the plasmid pLat52::AtSac9-mCherry-pEntry. For cloning of the plasmid pLat52::mcherry-pEntry, the mCherry sequence was amplified with 5'-Sall- and 3'-NotI sites and cloned as a Sall/NotI fragment into pLat52::pentryA.

A *StIPP*-RNAi fragment was cloned from cDNA using the primers 5'-CACCAACTTCGTCTCATCTTTGCATC-3' and 5'-CTTCTGATTAACCAACCCAATC-3'. The resulting 312 bp fragment was cloned into the pENTR<sup>TM</sup>/D-TOPO<sup>®</sup> vector and subsequently into the binary vector pHellsgate12 (Wesley *et al.*, 2001) by LR recombination. This was used for *Agrobacterium tumefaciens* AGL0-mediated transformation into *S. tuberosum* cv Désirée plants.

## Analysis of transcript abundance

RNA was isolated using Trizol reagent (Chomczynski & Sacchi, 1987). Briefly, 2 µg of RNA were used for DNaseI (Qiagen, Hilden, Germany) digestion and subsequent cDNA synthesis, using RevertAid (Thermo Fisher Scientific, Fermentas). Quantitative real-time polymerase chain reaction (qPCR) was performed with the Maxima Probe qPCR Master Mix (Thermo Fisher Scientific, Fermentas). Samples were run on an Mx3005P qPCR System (Agilent Technologies, Santa Clara, CA, USA). The following primers and real-time probes were used: StIPP: 5'-GGATTGGGTTGGTTAATCAGAA-3', 5'-AACCATTTGTATGCCCTTGTAGC-3' with Roche Universal Probe Library Probe no. 68; EF1α: 5'-CACTGCCAGGTCATCATC-3', 5'-GTCGAGCACTGGTGCATATC-3' and Roche Universal Probe Library Probe no. 162 (Roche, Basel, Switzerland).

## Expression of StIPP in *Escherichia coli* and preparation of protein samples

pDEST-N112-StIPP or the empty vector coding for maltose binding protein (MBP) only were transferred into *Escherichia coli* Rosetta gami cells. Protein expression was induced with 1 mM IPTG. After resuspension in the presence of lysozyme and Halt<sup>TM</sup> protease inhibitor cocktail (Thermo Fisher Scientific), cells were lysed by sonication and centrifuged. The cleared lysate was used for enzyme assays.

## Determination of StIPP activity

Enzyme activity was analyzed against different phosphoinositide and inositol polyphosphate substrates. Phosphoinositide substrates were obtained from Avanti Polar Lipids (Alabaster, AL, USA), including PtdIns3P (1,2-dioleoyl-sn-glycero-3-phospho-(1'-myo-inositol-3'-phosphate), PtdIns4P (1,2-dioleoyl-sn-glycero-3-phospho-1'-myo-inositol-4'-phosphate), PtdIns5P (1,2-dioleoyl-sn-glycero-3-phospho-1'-myo-inositol-5'-phosphate), PtdIns(3,5)P<sub>2</sub> (1,2-dioleoyl-sn-glycero-3-phospho-1'-myo-inositol-3',5'-bisphosphate), and PtdIns(4,5)P<sub>2</sub> (L-α-phosphatidylinositol-4,5-bisphosphate from porcine brain). Lipids were dissolved in 5 µl of 2% TritonX-100 in water and sonicated for 10 min on ice. The lipids were dissolved at 3–5 µg per reaction and mixed with 12.5 µl of lipid assay buffer (Ercetin & Gillaspay, 2004) and 7.5 µl of cleared lysate of MBP or StIPP, and the reactions were incubated for 2 h at room temperature. Lipids were extracted as previously described (Cho *et al.*, 1992) and separated by thin-layer chromatography (TLC) on HPTLC silica S60 plates (Merck, Darmstadt, Germany) with chloroform/methanol/ammonium hydroxide/water (50 : 50 : 4 : 11 (v/v/v/v)) as a developing solvent. The separated lipids were visualized as previously described (König *et al.*, 2008a).

To test the rephosphorylation of StIPP reaction products, extracted lipids were re-dissolved in 10 µl of 2%-TritonX-100 and added to a 30 µl reaction mixture containing 37.5 mM MgCl<sub>2</sub>; 2.5 mM NaMoO<sub>4</sub>; 2.5 mM ATP; and 1 µl γ[<sup>33</sup>P]-ATP; 3 mM Tris, pH 7.5. This mixture was split in two and each part added to

30  $\mu$ l enzyme solution, containing 0.15  $\mu$ g PIP4K2A (Sigma-Aldrich, Schnellendorf, Germany) or 0.2  $\mu$ g PIP5K1A (Sigma-Aldrich), respectively, in 30 mM Tris, pH 7.5. After incubation for 2 h at room temperature, lipids were extracted as described, redissolved in chloroform and separated by TLC on silica S60 plates (Merck). Phosphorus-33 ( $^{33}\text{P}$ )-incorporation was visualized with a phosphor imager system (BAS-1500; Fujifilm, Düsseldorf, Germany) and sensitive imager screens (BAS-MP 2040s; Fujifilm). High-performance liquid chromatography (HPLC) analysis of soluble inositol phosphates was performed as previously described (Stevenson-Paulik *et al.*, 2005), using a Dionex Ultimate 3000 System equipped with a strong anion exchange (SAX) column (Dionex/Thermo, Darmstadt, Germany).

### Cultivation and treatment of plants

Growth and treatment of potato plants (*S. tuberosum* cv Désirée) was performed as described (Dobritzsch *et al.*, 2016). *Nicotiana benthamiana* L. plants were grown in a glasshouse. For transient expression, 4-wk-old potato or 5-wk-old *N. benthamiana* plants were infiltrated with a suspension of *Agrobacterium tumefaciens* ( $\text{OD}_{600} = 0.1$ ) carrying different constructs. Three days after infiltration, fluorescence was visualized by confocal laser scanning microscopy (LSM 710; Carl Zeiss, Oberkochen, Germany). For transient expression with subsequent infection of detached transformed leaves, *N. benthamiana* plants were grown in phytochamber under long day conditions (16 h light,  $140 \mu\text{mol m}^{-2} \text{s}^{-1}$  at 20 °C and 60% relative humidity). Transient transformation and subsequent infection with the *P. infestans* isolate 88069 (kindly provided by Y. Dagdas) was carried out as described in Bozkurt *et al.* (2014).

### Transformation of tobacco pollen by particle bombardment

Mature pollen was collected from four to six flowers of 8-wk-old tobacco (*N. tabacum* L.) plants. Transient expression in pollen tubes was performed as previously described (Stenzel *et al.*, 2012).

### Confocal microscopy

Imaging was performed using LSM710 (Zeiss), LSM 780 (Zeiss) or LSM 880 Airyscan (Zeiss) confocal microscopes using  $\times 20$ ,  $\times 40$  air, and  $\times 63$  water-immersion objectives. Excitation and emission wavelengths were set as follows: GFP – excitation 488 nm, emission 495–550 nm, mCherry and RFP – excitation 561 nm, emission 571–624 nm). Colocalization images were taken using sequential scanning between lines. Image analysis was done with IMAGEJ (1.49b).

### Preparation and transient expression in Arabidopsis protoplasts

*Arabidopsis thaliana* L. mesophyll protoplasts were isolated and transformed with 10  $\mu$ g pUGW14-StIPP<sub>oS</sub>/100  $\mu$ l protoplasts or 1  $\mu$ g pUGW15-CFP/100  $\mu$ l protoplasts according to (Yoo

*et al.*, 2007). Transfected protoplasts were harvested 16 h later by centrifugation, the supernatant was removed and the cell pellets frozen in liquid nitrogen.

### Western blot

For standard western blot, protein extraction from protoplasts was done by direct application of Laemmli sodium dodecyl sulfate (SDS) sample buffer. Protein separation by SDS-PAGE (polyacrylamide gel electrophoresis) and immunoblotting on nitrocellulose membrane or polyvinylidene difluoride (PVDF) membrane were performed with standard protocols. Proteins were detected with anti-His, anti-FLS2, anti-mouse and anti-rabbit antibodies. For FLS2 signal quantification, a fluorescent western blot was performed combining the SPL Kit (NH DyeAGNOSTICS GmbH, Halle (Saale), Germany) and an IR-coupled antibody (Li-Cor Biosciences GmbH, Bad Homburg, Germany). Polyclonal rabbit antibodies against FLS2 were produced and affinity purified against the C-terminal peptide KANSFREDRNDREV (Immunoglobe) as previously described (Chinchilla *et al.*, 2006). For protein extraction, sample buffer (100 mM NaCl, 20 mM DTT, 0.1% Triton X-100, 0.1% SDS, 0.1% NP-40, 50 mM Tris pH 9.6, 1 mM PMSF, 1 $\times$  Halt Protease Inhibitor Cocktail (Thermo Fisher Scientific)) was added to protoplasts. SPL sample buffer was added according to the manufacturer's instructions. The samples were incubated at 65°C for 15 min and centrifuged for 15 min at 21 130 g. Protein separation was done with 8%-SDS-PAGE. Afterwards, the gel was separated at the size of 63 kDa and the detection of total protein and the provided standard was performed with a laser scanner (Typhoon FLA 9500; GE Healthcare, Freiburg, Germany) according to the SPL kit manufacturer's instructions.

## Results

*StIPP* was identified in microarray analyses as a transcript accumulating in response to treatment by Pep-13 in wild type potato plants as well as in transgenic potato plants impaired in biosynthesis (*StAOC*-RNAi and *StOPR3*-RNAi) or perception (*StCOI1*-RNAi) of jasmonic acid (Halim *et al.*, 2009). The 60mer on the potato chips (Kloosterman *et al.*, 2008) corresponds to gene locus PGSC0003DMG400016891, annotated to encode an inositol polyphosphate phosphatase (<http://solanaaceae.plantbiology.msu.edu/>). In this study, the *StIPP* protein is characterized *in vitro* and *in vivo* to elucidate its roles in the defense of potato against *P. infestans*.

*StIPP* is a Pep-13-activated gene with similarity to sequences for inositol polyphosphate phosphatases

The coding region of the *StIPP* gene covers eight exons and is 1017 bp in length (Fig. 1a). The deduced gene product of 338 amino acids (Sotub04g033080.1.1; XP\_006366454.1) displays 58% sequence identity to the Arabidopsis inositol polyphosphate 5-phosphatase At5PTase11 encoded by the gene locus *At1g47510* and includes motifs relevant for phosphatase function

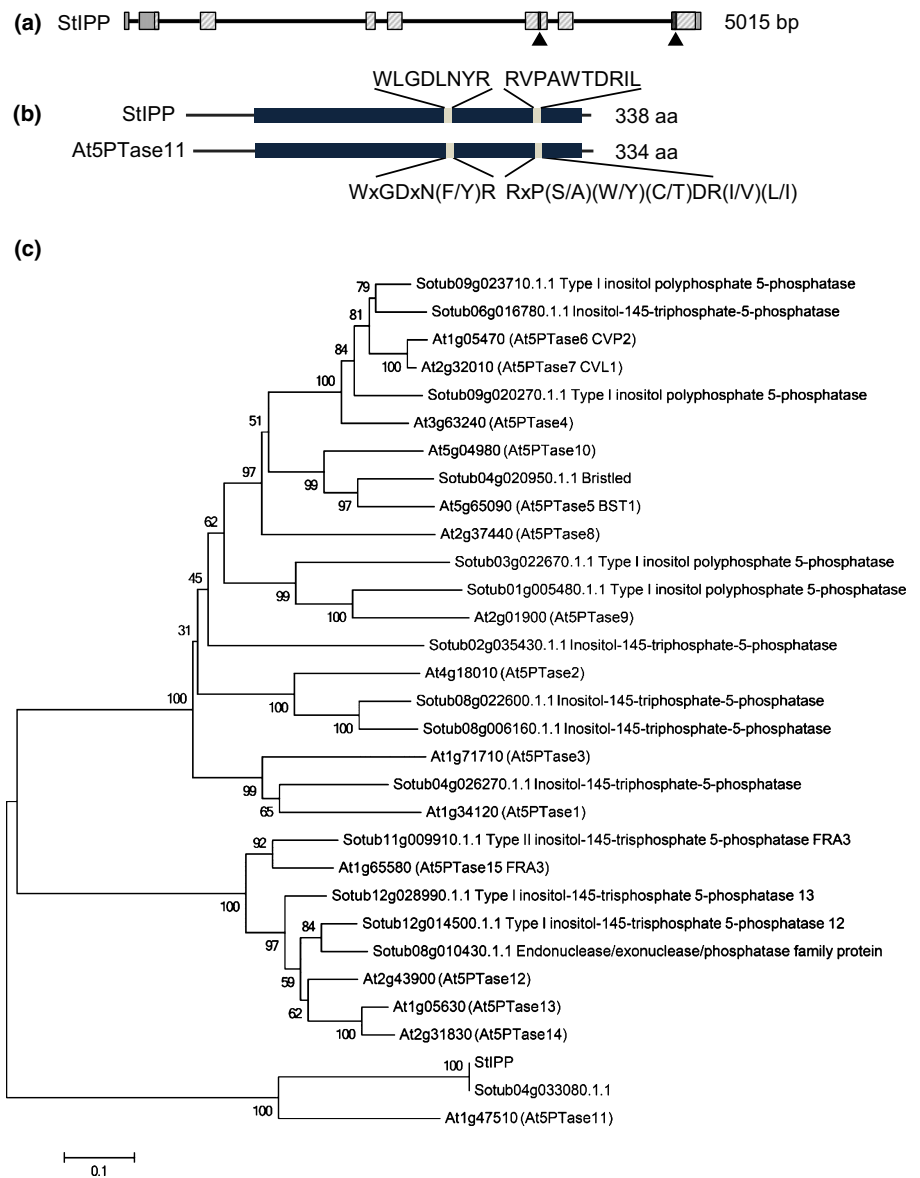


**Fig. 1** *StIPP* is a gene with similarity to sequences for inositol polyphosphate phosphatases. (a) Exon-intron structure of the *StIPP* gene from potato (*Solanum tuberosum*). Boxes indicate exons, hatched boxes mark the predicted catalytic domain. The coding regions of amino acid motifs conserved in inositol polyphosphate phosphatases (IPPs) are indicated by the arrowheads. (b) Domain structure of the deduced *StIPP* protein. *StIPP* structure is compared to that of the closest homolog in Arabidopsis, *At5PTase11*. The sequences indicate the IPP recognition motifs for *StIPP* (upper panel) and those found in Arabidopsis 5-PTases (lower panel). (c) Phylogenetic relations of *StIPP*, its closest homologs and the corresponding Arabidopsis genes are shown. The evolutionary history was inferred using the neighbor-joining method (Saitou & Nei, 1987). The optimal tree with the sum of branch length = 5.94410666 is shown. The percentage of replicate trees in which the associated taxa clustered together in the bootstrap test (1000 replicates) are shown next to the branches (Felsenstein, 1985). The tree is drawn to scale, with branch lengths in the same units as those of the evolutionary distances used to infer the phylogenetic tree. The evolutionary distances were computed using the Poisson correction method (Zuckerkandl & Pauling, 1965) and are in the units of the number of amino acid substitutions per site. The analysis involved 31 amino acid sequences. All positions containing gaps and missing data were eliminated. There was a total of 200 informative positions in the final dataset. Evolutionary analyses were conducted using MEGA6 (Tamura *et al.*, 2011).

(Fig. 1b) (Majerus & York, 2009). Phylogenetic analysis confirms association of *StIPP* with a well-funded clade, which also includes the sequence for *At5PTase11* (Fig. 1c).

The up to 10-fold accumulation of *StIPP* transcript determined by microarray analyses for potato leaves treated with Pep-13 was independent of oxo-phytodienoic acid or jasmonic acid (Fig. 2a). Pep-13-dependent activation of *StIPP* was verified by independent qRT-PCR experiments, and Pep-13 treatment resulted in significantly enhanced *StIPP* transcript levels as early as 1 h after Pep-13 infiltration, compared to the transcript levels of leaves infiltrated with the inactive W2A-peptide (Fig. 2b), and *StIPP* transcript levels continued to increase after 24 h. Pep-13-induced accumulation of *StIPP* transcripts was also observed in potato leaves infected with *P. infestans* (Fig. 2c) and after wounding (Fig. 2d), with significantly enhanced *StIPP* transcript levels detectable after 1 d and 6 h, respectively. Together, the data indicate that the *StIPP* gene is induced in potato leaves upon PAMP treatment, pathogen infection and wounding.

***StIPP* is an inositol polyphosphate 5-phosphatase specific for PtdIns(4,5)P<sub>2</sub>**

For biochemical characterization of the *StIPP* gene product, the *StIPP* coding region was cloned into the bacterial expression vector pDEST-N112-MBP (Dyson *et al.*, 2004) encoding a translational fusion of *StIPP* to an N-terminal MBP and a His-tag, as was previously used for the expression of phosphoinositide-modifying enzymes (Ischebeck *et al.*, 2008; Stenzel *et al.*, 2008, 2012; Hempel *et al.*, 2017). Transformation of Rosetta gami cells with the *StIPP* expression construct resulted in bacterial lysates that contained soluble MBP-*StIPP* fusion protein of calculated *c.* 83 kDa, as determined by western blot analyses using anti-His antibodies (Fig. 3a). Catalytic activity and substrate preference were determined by incubation of lysates containing MBP or MBP-*StIPP* with different phosphoinositide substrates, subsequent lipid extraction and the analysis of the hydrophobic reaction products by TLC and CuSO<sub>4</sub>-staining (Fig. 3b). In these

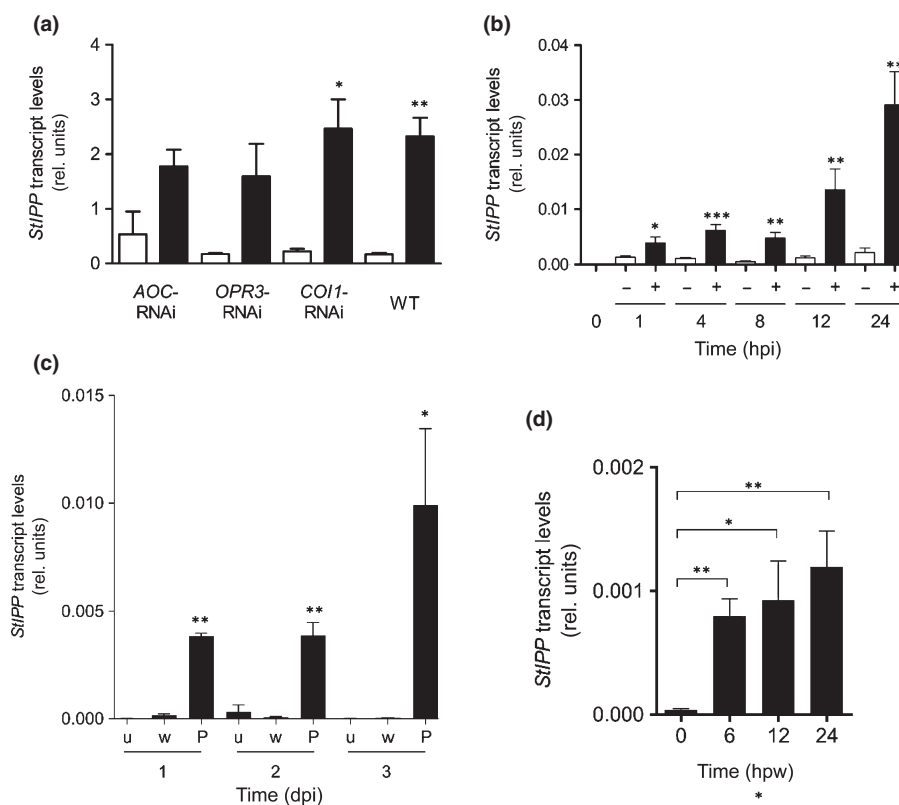


**Fig. 2** Expression of *StIPP* is induced by Pep-13 infiltration, *Phytophthora infestans* and wounding. The induction of the *StIPP* gene by relevant stresses was analyzed by transcript array analysis and confirmed by quantitative real time RT-PCR. (a) Transcript array data for wild type (WT) potato plants or transgenic potato plants expressing RNAi constructs against the genes encoding potato allene oxide cyclase (*StAOC*), 12-oxophytodienoic acid reductase 3 (*StOPR3*) or coronatine insensitive 1 (*StCOI1*) infiltrated with W2A (open bars) or Pep-13 (closed bars), as indicated. The array was performed with cDNA from RNA isolated 8 h after treatment ( $n = 3$ , three independent experiments). (b–d) WT potato plants were subjected to PAMP-treatment (b), to infection with *P. infestans* (c) or to wounding (d), RNA was isolated at the time points indicated, reverse transcribed and *StIPP* transcript levels were determined by quantitative real time RT-PCR using *StEF1 $\alpha$*  as a reference. (b) *StIPP* transcript changes upon infiltration with W2A (white bars) or Pep-13 (black bars) ( $n \geq 5$ , three independent experiments). (c) *StIPP* transcript changes upon infection with *P. infestans* CRA208m2 (Si-Ammour *et al.*, 2003). Plants were either untreated (u) or infected by applying 10  $\mu$ l droplets of water (w) or a *P. infestans* zoospore suspension ( $10^5$  zoospores  $\text{ml}^{-1}$ ) to the abaxial side of the leaves (P;  $n \geq 4$ , two independent experiments). (d) *StIPP* transcript changes upon wounding of leaves of WT potato plants with a hemostat ( $n \geq 7$ , three independent experiments). Error bars represent SEM. Statistical analyses were performed using a Student's *t*-test ((a, b) W2A vs Pep-13; Mann Whitney *U*-test (c, d) treatment vs control). Asterisks indicate statistical differences (\*,  $P \leq 0.05$ ; \*\*,  $P \leq 0.01$ ; \*\*\*,  $P \leq 0.001$ ). hpi, hours post infection; dpi, days post infection; hpw, hours post wounding.

assays, recombinant MBP-*StIPP* protein specifically converted  $\text{PtdIns}(4,5)\text{P}_2$  to a phosphatidylinositol-monophosphate (Fig. 3b). None of the additionally tested phosphoinositide substrates were converted by MBP-*StIPP* *in vitro*, including phosphatidylinositol 3,5-bisphosphate ( $\text{PtdIns}(3,5)\text{P}_2$ ), phosphatidylinositol 3-phosphate ( $\text{PtdIns}3\text{P}$ ),  $\text{PtdIns}4\text{P}$  or phosphatidylinositol 5-phosphate ( $\text{PtdIns}5\text{P}$ ). Moreover, other tested substrates were not converted by lysates containing MBP alone (Fig. 3b), confirming that *E. coli* does not harbor enzyme activities converting phosphoinositides, as was previously reported (Ischebeck *et al.*, 2008; Stenzel *et al.*, 2008). As some inositol polyphosphate phosphatases have previously been demonstrated to not only dephosphorylate lipid substrates but also accept soluble inositol polyphosphates, MBP controls and MBP-*StIPP* were also tested against a range of soluble inositol polyphosphates, and the reaction products analyzed by HPLC coupled with non-labeled colorimetric metal dye-detection (Stevenson-Paulik *et al.*, 2005). In these assays, no hydrolysis of  $\text{Ins}(1,3,5)\text{P}_3$ ,  $\text{Ins}(1,3,4,5)\text{P}_4$ ,  $\text{Ins}(1,4,5)\text{P}_3$ ,  $\text{Ins}(1,4,5,6)\text{P}_4$ ,  $\text{Ins}(1,3,4,5,6)\text{P}_5$  or  $\text{Ins}$

$(1,2,3,4,5,6)\text{P}_6$  was detected for MBP, nor for MBP-*StIPP* *in vitro* (Supporting information Fig. S1). Together, these results indicate that *StIPP* is a functional phosphoinositide phosphatase with an unusually high substrate specificity for a single phosphoinositide substrate, preferentially hydrolyzing  $\text{PtdIns}(4,5)\text{P}_2$  to a  $\text{PtdIns}$ -monophosphate.

Dephosphorylation of  $\text{PtdIns}(4,5)\text{P}_2$  by *StIPP* can occur either at the D4 or the D5 phosphate, respectively yielding either  $\text{PtdIns}5\text{P}$  or  $\text{PtdIns}4\text{P}$ . To determine the regioselectivity of the *StIPP*-mediated dephosphorylation,  $\text{PtdIns}(4,5)\text{P}_2$  was incubated with recombinant MBP-*StIPP* protein, and the reaction product was subsequently isolated and used as a substrate for re-phosphorylation assays. These assays were performed in the presence of  $\gamma$  [ $^{33}\text{P}$ ]ATP and either commercial human  $\text{PI}4\text{P}$  5-kinase or human  $\text{PI}5\text{P}$  4-kinase, which specifically act on  $\text{PtdIns}4\text{P}$  or  $\text{PtdIns}5\text{P}$  substrates, respectively. The specificity of these helper enzymes was first confirmed *in vitro* by converting the respective substrates,  $\text{PtdIns}4\text{P}$  and  $\text{PtdIns}5\text{P}$  (Fig. 3c). While both human enzymes were active as expected, re-phosphorylation of the *StIPP*

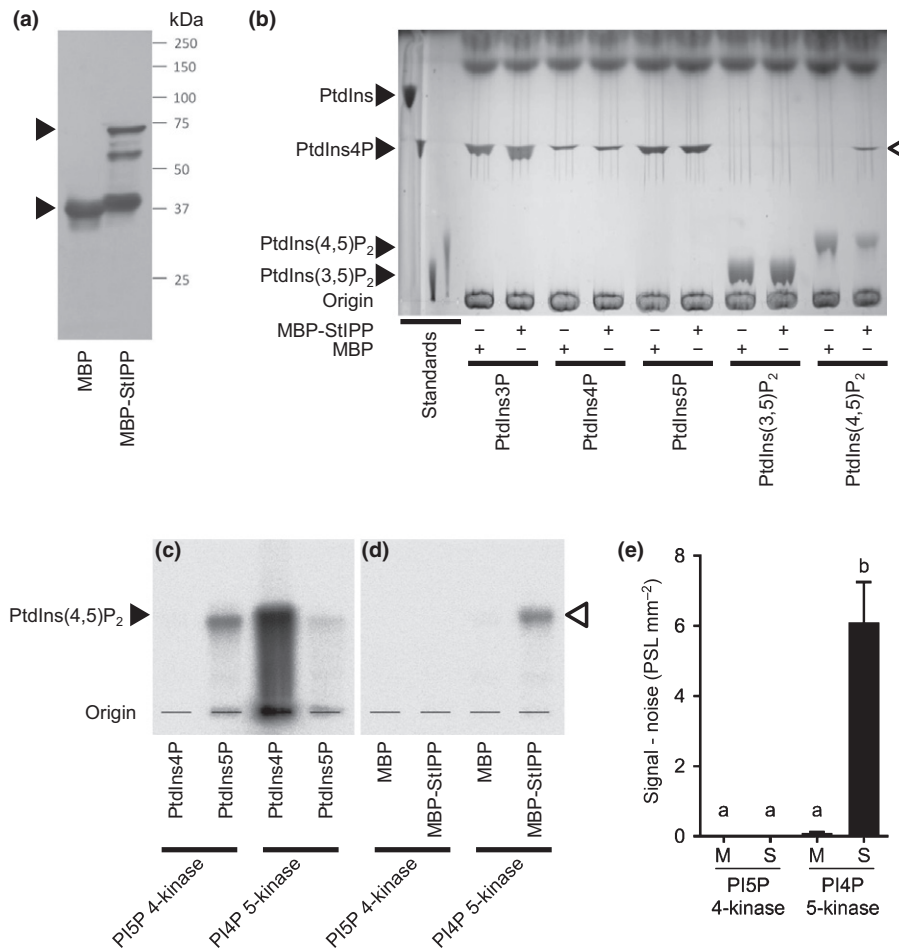


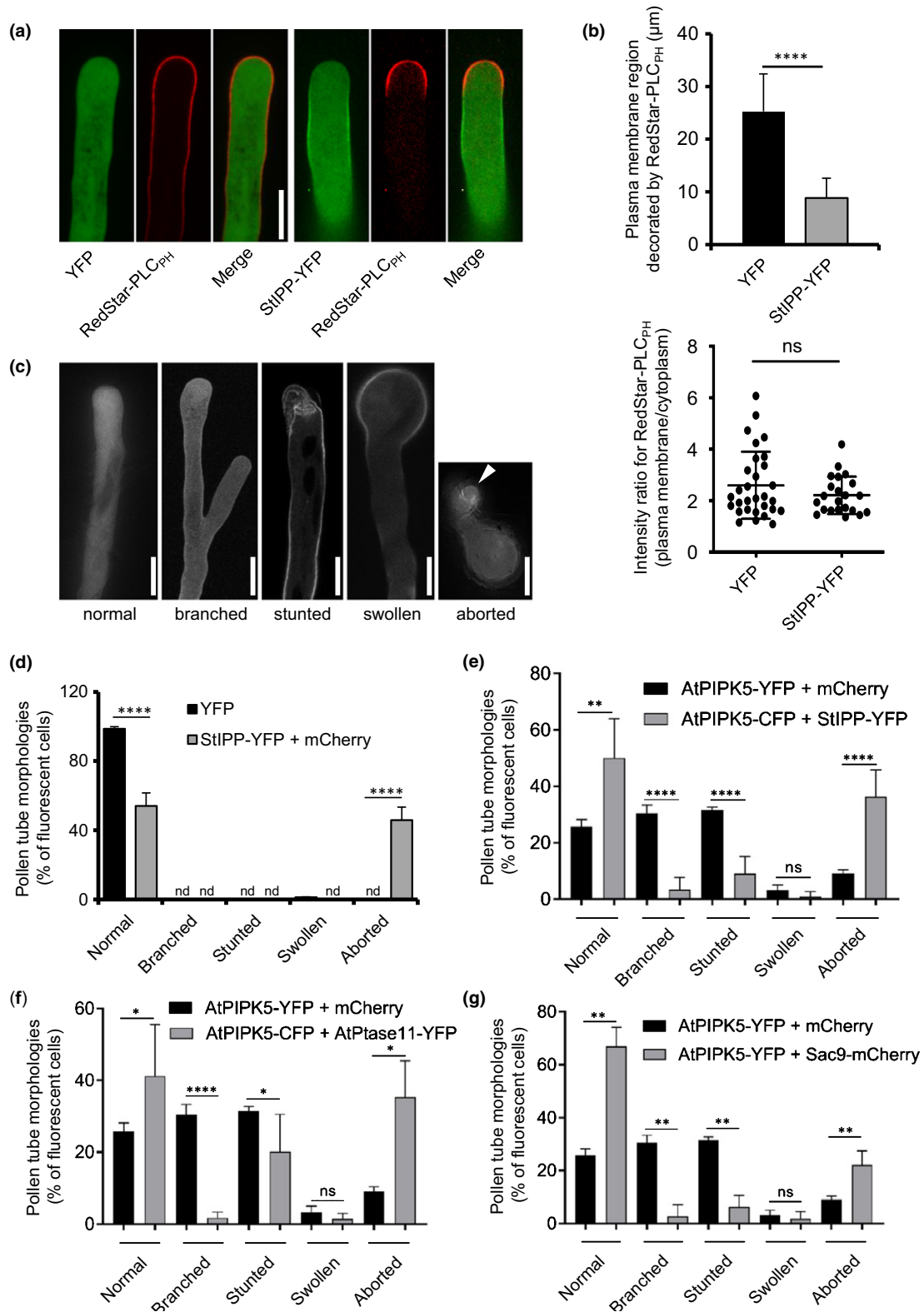
**Fig. 3** StIPP is an inositol polyphosphate 5-phosphatase specific for PtdIns(4,5)P<sub>2</sub>. The catalytic activity, substrate preference and regiospecificity of the StIPP gene product was determined *in vitro*. (a) Lysates of *Escherichia coli* expressing maltose binding protein (MBP) or the MBP-StIPP fusion protein (calculated molecular mass 83 kD) were subjected to western blot analysis. Arrowhead indicate the migration of the recombinant MBP and MBP-StIPP proteins. (b) Lysates of *E. coli* cells expressing MBP or MBP-StIPP were incubated with phospholipid substrates, as indicated. The reaction products were re-extracted, separated by thin-layer chromatography, visualized by staining with copper sulfate (CuSO<sub>4</sub>) and identified according to comigration with authentic lipid standards, as indicated. The result shown is representative for three independent experiments. The open arrowhead indicates the migration of the reaction product of PtdIns(4,5)P<sub>2</sub> hydrolysis, a PtdIns-monophosphate. (c–e) To determine the regiospecificity of the dephosphorylation of PtdIns(4,5)P<sub>2</sub>, the PtdIns-monophosphate reaction product was re-extracted and subjected to a rephosphorylation assay. Rephosphorylation was catalyzed in the presence of  $\gamma$ [<sup>33</sup>P]ATP by commercially available recombinant human PI5P 4-kinase or PI4P 5-kinase, respectively, and visualized by phosphor imaging. (c) Control experiments performed against authentic PtdIns4P and PtdIns5P substrates indicate the specificity of the human enzymes for their respective substrates. (d) Reaction products of StIPP-mediated PtdIns(4,5)P<sub>2</sub> hydrolysis were subjected to rephosphorylation by either human PI5P 4-kinase or by human PI4P 5-kinase, as indicated. The open arrowhead indicates the migration of PtdIns(4,5)P<sub>2</sub> formed by human PI4P 5-kinase, but not by PI5P 4-kinase. (e) Quantification of the radioactivity shown in (d) was performed using TINA software (Raytest). M, MBP; S, MBP-StIPP. Data shown are means  $\pm$  SD from three replicates in one experiment. Statistical analyses were performed using one-way analysis of variance. Different letters indicate significant differences. Experiments shown in (c) and (d) were performed twice, with four replicates, with similar results. PtdIns, phosphatidylinositol; PtdIns3P, phosphatidylinositol 3-phosphate; PtdIns4P, phosphatidylinositol 4-phosphate; PtdIns5P, phosphatidylinositol 5-phosphate; PtdIns(3,5)P<sub>2</sub>, phosphatidylinositol 3,5-bisphosphate; PtdIns(4,5)P<sub>2</sub>, phosphatidylinositol 4,5-bisphosphate.

reaction product was only observed with the PI4P 5-kinase (Fig. 3d), identifying the reaction product of MBP-StIPP-mediated conversion of PtdIns(4,5)P<sub>2</sub> as PtdIns4P. A quantification of the re-phosphorylation results is shown in Fig. 3(e). The *in vitro* data indicate that the StIPP protein acts as a PtdIns(4,5)P<sub>2</sub>-specific 5-phosphatase producing PtdIns4P.

### StIPP is functional *in vivo*

As recombinant StIPP used PtdIns(4,5)P<sub>2</sub> *in vitro* as a substrate, we next addressed whether the expression of StIPP would

influence PtdIns(4,5)P<sub>2</sub> also *in vivo*. For this purpose, we first used tobacco pollen tubes, which represent a well-characterized model to assess phosphoinositide-dependent membrane trafficking defects (Ischebeck *et al.*, 2008, 2010; Sousa *et al.*, 2008; Stenzel *et al.*, 2012; Hempel *et al.*, 2017). A fluorescent biosensor for PtdIns(4,5)P<sub>2</sub>, RedStar-PLC<sub>PH</sub> (Ischebeck *et al.*, 2008), decorated a well-defined subapical plasma membrane region of pollen tubes when coexpressed with YFP as a control protein (Fig. 4a, left panels). By contrast, coexpression of RedStar-PLC<sub>PH</sub> with StIPP-YFP under identical conditions resulted in a substantially reduced dimension of the plasma membrane region decorated by



RedStar-PLC<sub>PH</sub> (Fig. 4a, right panels). This pattern is consistent with an *in vivo* function of the StIPP protein as a PtdIns(4,5)P<sub>2</sub>-specific phosphatase as determined *in vitro* (Fig. 3). The StIPP-YFP fusion localized to the subapical plasma membrane of the pollen tube cells (Fig. 4a, right panels) in a pattern similar to that

shown by intrinsic tobacco enzymes hydrolyzing PtdIns(4,5)P<sub>2</sub>, such as NtPLC3 (Helling *et al.*, 2006; Stenzel *et al.*, 2020). Quantification of the dimensions of the plasma membrane region occupied by RedStar-PLC<sub>PH</sub> indicates a significant reduction upon coexpression of StIPP-YFP ( $n=30$  cells for YFP;  $n=20$

**Fig. 4** StIPP-YFP impacts on PtdIns(4,5)P<sub>2</sub> *in vivo* and antagonizes PtdIns(4,5)P<sub>2</sub>-dependent effects on cell morphologies in tobacco pollen tubes. The *in vivo* function of StIPP was assessed upon transient expression in tobacco (*Nicotiana tabacum*) pollen tubes. (a) Effects of StIPP on PtdIns(4,5)P<sub>2</sub> were assessed *in vivo* by monitoring the distribution of RedStar-PLC<sub>PH</sub>, a fluorescent biosensor for PtdIns(4,5)P<sub>2</sub>. The RedStar-PLC<sub>PH</sub> reporter decorated a subapical plasma membrane region when coexpressed with a YFP control (left panels). The dimension of the plasma membrane region occupied by RedStar-PLC<sub>PH</sub> was reduced upon coexpression with StIPP-YFP (right panels). (b) Quantification of the dimension of the plasma membrane region (distance of the lower edge from the tip) decorated by RedStar-PLC<sub>PH</sub> upon coexpression with YFP or with StIPP-YFP, as indicated (upper panel). Ratio of plasma membrane vs cytosolic fluorescence of RedStar-PLC<sub>PH</sub> upon coexpression with YFP or with StIPP-YFP, as indicated. Data are the mean  $\pm$  SD from 30 and 20 experiments, respectively. (c) Polar tip growth of pollen tubes is sensitive to perturbation of PtdIns(4,5)P<sub>2</sub> production, giving rise to aberrant cell shapes. Pollen tube morphologies that have previously been reported include normal growth, here upon expression of a YFP control; branched growth, here upon expression of the PI4P 5-kinase PIP5K5 (the image is a three-dimensional projection of a confocal image stack); stunted growth, here upon strong expression of PIP5K5 (with apical membrane infolding); tip swelling, here upon expression of PIP5K11; and aborted growth, here upon expression of StIPP-YFP, where expansion of the pollen tube apex (arrowhead) ceases immediately upon emergence from the pollen grain. These cell morphologies were scored to assess the impact of StIPP on PI4P 5-kinase-mediated defects. (d) Control experiments illustrating cell morphologies observed upon expression of YFP or of coexpressed StIPP-YFP and mCherry, as indicated. The expression of StIPP-YFP resulted in an increased incidence of aborted pollen tubes. Data represent 76 cells for YFP and 88 cells for StIPP-YFP/mCherry. (e) An antagonistic function of StIPP-YFP towards PtdIns(4,5)P<sub>2</sub>-dependent effects was tested *in vivo* by coexpressing the Arabidopsis PI4P 5-kinase AtPIP5K5 with either a fluorescent protein alone (black bars) or with StIPP-YFP (gray bars) and scoring the resulting cell morphologies. Data represent 86 cells for PIP5K5-YFP/mCherry and 92 cells for PIP5K5-CFP/StIPP-YFP. Cell morphologies were categorized as normal, branched, stunted, swollen or aborted, as indicated. (f, g) Control experiments were performed in which the effects of bona fide PtdIns(4,5)P<sub>2</sub>-specific lipid phosphatases were tested, such as AtPTase11 (f) or Sac9 (g). Data represent 86 cells for PIP5K5-YFP/mCherry and 78 cells for PIP5K5-CFP/AtPTase11-YFP (d) or 86 cells for PIP5K5-YFP/mCherry and 96 cells for PIP5K5-CFP/Sac9-YFP (e). Data in panels (d–g) represent means  $\pm$  SD. Statistical analyses were performed using unpaired two-tailed Student's *t*-tests. Asterisks indicate statistical differences, as indicated (\*,  $P \leq 0.05$ ; \*\*,  $P \leq 0.01$ ; \*\*\*\*,  $P \leq 0.0001$ ). ns, not significant. Bars, 10  $\mu$ m.

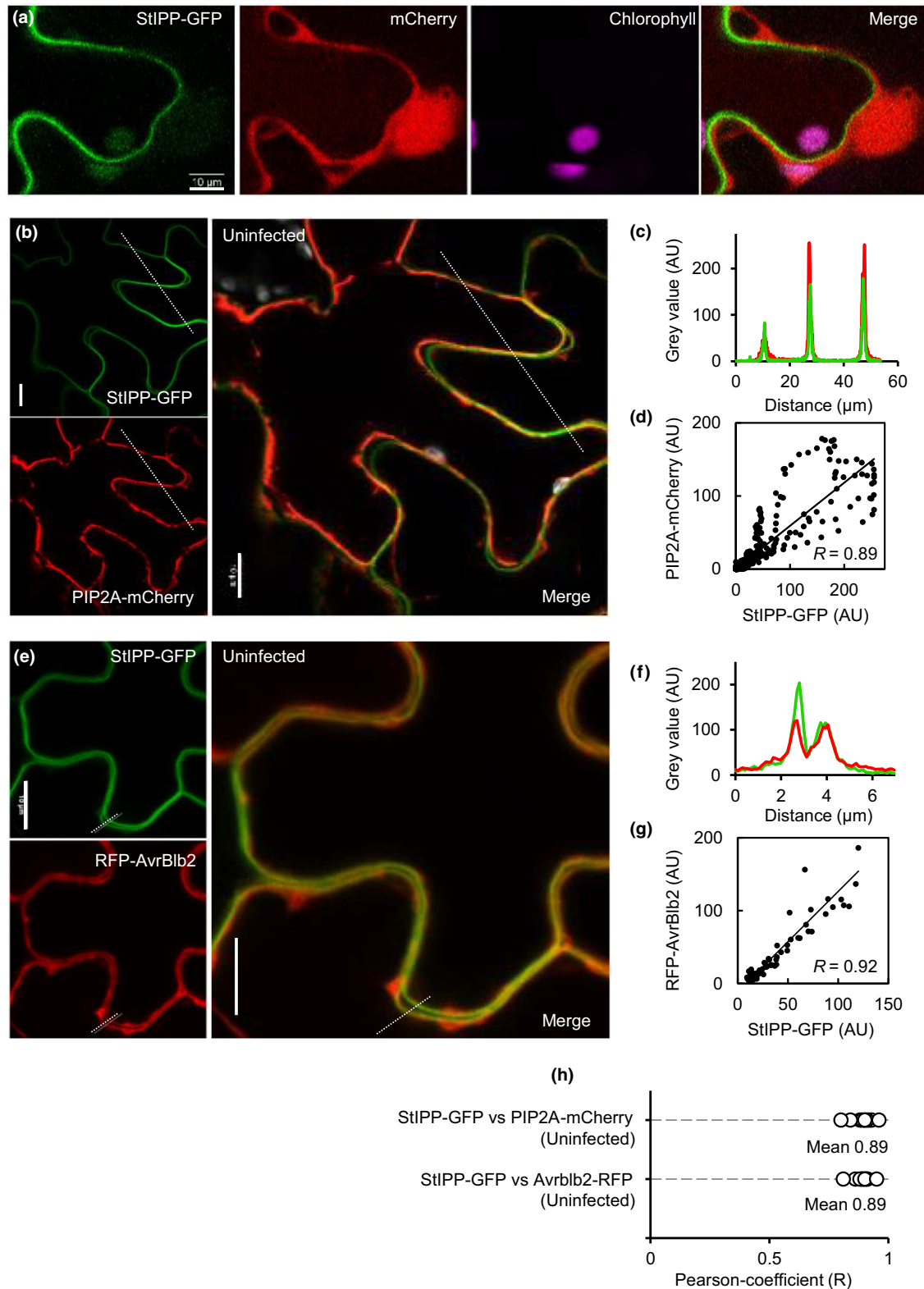
cells for StIPP-YFP;  $P \leq 0.0001$ ) (Fig. 4b, top). The proportion of plasma membrane-associated and cytosolic RedStar-PLC<sub>PH</sub> fluorescence did not significantly change upon expression of StIPP-GFP compared to values upon expression of YFP (Fig. 4b, bottom). Overall, the data are consistent with an *in vivo* effect of expressed StIPP-YFP on PtdIns(4,5)P<sub>2</sub> accumulation in tobacco pollen tubes.

To further test whether the expression of StIPP would interfere with PtdIns(4,5)P<sub>2</sub>-dependent aspects of pollen tube growth *in vivo*, we assessed the impact of StIPP-YFP expression on pollen tube cell morphologies arising from the modulation of PtdIns(4,5)P<sub>2</sub>. Pollen tubes display characteristic cell morphologies upon overproduction of PtdIns(4,5)P<sub>2</sub>, which can easily be scored, including pollen tubes with branched or stunted tips (Ischebeck *et al.*, 2008, 2010; Stenzel *et al.*, 2012; Hempel *et al.*, 2017) or displaying tip swelling (Ischebeck *et al.*, 2011; Stenzel *et al.*, 2012, 2020). The range of pollen tube morphologies observed is represented in Fig 4(c), as indicated. The expression of StIPP-YFP alone in pollen tubes resulted in a significantly increased proportion of cells in which pollen tube growth was aborted shortly after tubes emerged from the pollen grains, whereas pollen tube growth was not affected by expression of the YFP control ( $n = 76$  cells for YFP;  $n = 88$  cells for StIPP-YFP/mCherry;  $P \leq 0.0001$ ) (Fig. 4d). To test whether StIPP-YFP expression interfered with PtdIns(4,5)P<sub>2</sub>-dependent processes, the morphological defects caused by the overexpression of the PI4P 5-kinase, PIP5K5 (Ischebeck *et al.*, 2008), were assessed during coexpression of PIP5K5-YFP with an mCherry control or during coexpression of PIP5K5-CFP with StIPP-YFP (Fig. 4e). The data indicate that the PIP5K5-CFP-dependent tip-branching and stunted morphologies were each significantly alleviated by the coexpression of StIPP-YFP, as compared to the effects of a coexpressed mCherry control (Fig. 4e), resulting in an increased number of normal growing pollen tubes when both PIP5K5-CFP and StIPP-YFP were present ( $n = 86$  cells for PIP5K5-YFP/

mCherry;  $n = 92$  cells for PIP5K5-CFP/StIPP-YFP;  $P \leq 0.01$ ). The patterns obtained for the coexpression of PIP5K5-CFP with StIPP-YFP suggest that StIPP can functionally antagonize PIP5K5. The patterns furthermore resemble those obtained for coexpression of PIP5K5 with other PtdIns(4,5)P<sub>2</sub>-specific 5-phosphatases from Arabidopsis, such as AtPIP5K5-CFP vs At5PTase11-YFP (Ercetin *et al.*, 2008) ( $n = 86$  cells for PIP5K5-YFP/Cherry;  $n = 78$  cells for PIP5K5-CFP/PTase11-YFP;  $P \leq 0.05$ ) (Fig. 4f), or AtPIP5K5-YFP vs Sac9-mCherry (Williams *et al.*, 2005) ( $n = 86$  cells for PIP5K5-YFP/mCherry;  $n = 96$  cells for PIP5K5-CFP/Sac9-mCherry;  $P \leq 0.01$ ) (Fig. 4g), which is consistent with the *in vitro* characterization of potato StIPP as a PtdIns(4,5)P<sub>2</sub>-specific 5-phosphatase (Fig. 3). Together, the data indicate that StIPP-YFP localizes to the plasma membrane and antagonizes effects of PtdIns(4,5)P<sub>2</sub>-overproduction on pollen tube cell morphologies *in vivo*.

#### StIPP-GFP localizes to the plasma membrane of uninfected pavement cells of potato and *N. benthamiana*

Based on the results so far, we next investigated the subcellular localization of a StIPP-GFP fusion in vegetative plant tissues. StIPP-GFP was transiently expressed, in an initial experiment, in potato leaves under the control of the cauliflower mosaic virus (CaMV) 35S promoter (Fig. 5a). Coexpression with an mCherry control indicates plasma membrane localization of StIPP-GFP (Fig. 5a). To enable the coexpression with additional fluorescence markers, further characterizations were performed upon expression of StIPP-GFP in *N. benthamiana* leaves (Fig. 5b–h). Plasma membrane localization of StIPP-GFP was assessed for uninfected *N. benthamiana* pavement cells relative to the coexpressed plasma membrane aquaporin, PLASMA MEMBRANE INTRINSIC PROTEIN 2A (PIP2A) (Johanson *et al.*, 2001) fused to mCherry (Fig. 5b). Quantification of fluorescence intensities of the two markers along the dashed line in Fig. 5(b) indicates close



colocalization of the markers (Fig. 5c) with a Pearson coefficient ( $R$ ) for the colocalization of 0.89 (Fig. 5d). The localization of StIP-P-GFP was also analyzed relative to that of the fluorescence-tagged pathogen effector, RFP-AvrB1b2 (Fig. 5e,f). This effector was previously shown to localize at the plasma membrane upon

expression in epidermal *N. benthamiana* cells, and to re-localize to the extrahaustorial membrane (EHM) upon *P. infestans* infection (Bozkurt *et al.*, 2011, 2015). In uninfected cells, StIP-P-GFP showed a distinct plasma membrane signal at the cell periphery, where it co-localized with RFP-AvrB1b2 (Fig. 5e,f), with a high

**Fig. 5** StIPP-GFP localizes to the plasma membrane of uninfected epidermal cells of potato and tobacco leaves. The subcellular localization of a fluorescence-tagged StIPP variant was analyzed upon Agrobacterium-mediated transient expression in epidermal cells of potato or tobacco (*Nicotiana benthamiana*) leaves. (a) StIPP was transiently expressed as a GFP fusion protein in potato leaves, together with a cytoplasmic mCherry marker. Images were recorded three days after infiltration. (b) Coexpression of StIPP-GFP with the plasma membrane marker PIP2A-mCherry in non-infected *N. benthamiana* leaves. (c) Fluorescence intensity profiles recorded along the dashed line in (b), indicating colocalization of StIPP-GFP (green) with PIP2A-mCherry (red). (d) Correlation analysis of the fluorescence intensities recorded in (c) and corresponding Pearson coefficient. (e) Coexpression of StIPP-GFP with the *Phytophthora infestans* effector protein RFP-AvrBlb2 in uninfected *N. benthamiana* leaves. (f) Fluorescence intensity profiles recorded along the dashed line in (e), indicating colocalization of StIPP-GFP (green) with RFP-AvrBlb2 (red). (g) Correlation analysis of the fluorescence intensities recorded in (f) and corresponding Pearson coefficient. (h) Pearson coefficients for the colocalization of StIPP-GFP with PIP2A-mCherry or with RFP-AvrBlb2 were determined for 10 experiments, respectively, indicating a consistently high degree of colocalization patterns for these markers (0, no correlation; 1, perfect correlation). All markers were expressed under the control of the CaMV 35S promotor. The uninfected controls shown in this figure were mock-treated with water. AU, arbitrary units; bars, 10  $\mu$ m.

degree of colocalization indicated by the  $R=0.92$ . Pearson coefficients for the colocalization of StIPP-GFP with PIP2A-mCherry or with RFP-AvrBlb2 were determined for 10 experiments, each, and indicate a consistently high degree of colocalization of StIPP-GFP at the plasma membrane of uninfected pavement cells with either marker (Fig. 5h).

### StIPP-GFP relocates to pathogen entry sites upon infection

The localization of coexpressed StIPP-GFP and RFP-AvrBlb2 was further analyzed in epidermal cells of *N. benthamiana* upon infection with *P. infestans* 88069. After 3–4 d post infection (dpi), StIPP-GFP displayed clear association with the haustorium (Fig. 6a–c). In cells coexpressing StIPP-GFP and RFP-AvrBlb2, infection with *P. infestans* resulted in a re-localization of both StIPP-GFP and RFP-AvrBlb2 from the plasma membrane to the infection sites and developing EHM, with some retained plasma membrane association observed for either marker (Fig. 6d,g). In the majority of cases (52 out of 79 cells analyzed), StIPP-GFP but not RFP-AvrBlb2 retained a pronounced plasma membrane localization. Colocalization was consistently observed at the EHM, as is illustrated by the intensity plots (Fig. 6e) and the corresponding colocalization analysis (Fig. 6f). In a smaller number of cases (16 out of 79 cells analyzed), both StIPP-GFP and RFP-AvrBlb2 retained a similar degree of plasma membrane association in addition to localizing to the EHM (Fig. 6g), as illustrated by the intensity plots (Fig. 6h) and corresponding colocalization coefficient (Fig. 6i). Pearson coefficients for the colocalization of StIPP-GFP with RFP-AvrBlb2 were determined for 10 experiments and indicate a consistently high degree of colocalization of StIPP-GFP with RFP-AvrBlb2, regardless of whether the colocalization was analyzed globally or with a focus on the EHM (Fig. 6j). The patterns suggest that StIPP-GFP and RFP-AvrBlb2 are re-localizing from the plasma membrane to the EHM. As plasma membrane association of StIPP-GFP and RFP-AvrBlb2 appears to be retained independently, it appears possible that the markers may follow independent modes of relocation to the EHM.

### StIPP-GFP may act on PtdIns(4,5)P<sub>2</sub> specifically at infection sites

As StIPP specifically hydrolyzed PtdIns(4,5)P<sub>2</sub> to PtdIns4P *in vitro* and associated with *P. infestans* infection sites *in vivo*, we

next tested the subcellular localization of StIPP-GFP in relation to fluorescent reporters for PtdIns(4,5)P<sub>2</sub> or PtdIns4P in uninfected and infected tobacco leaf epidermis cells (Fig. 7). PtdIns(4,5)P<sub>2</sub> and PtdIns4P can be visualized *in vivo* by monitoring the subcellular distribution of the fluorescent reporters mCherry<sub>PLC-PH</sub> (van Leeuwen *et al.*, 2007; Simon *et al.*, 2014) or mCherry<sub>FAPP1-PH</sub> (Mishkind *et al.*, 2009; Simon *et al.*, 2014), respectively. In uninfected cells, the PtdIns(4,5)P<sub>2</sub>-biosensor mCherry<sub>PLC-PH</sub> localized to the cytosol, the nucleus (n) and the plasma membrane, where it colocalized with StIPP-GFP (Fig. 7a), as illustrated by the representative intensities (Fig. 7b) recorded along the dashed line in Fig. 7(a), with a colocalization coefficient for StIPP-GFP and mCherry<sub>PLC-PH</sub> in uninfected cells of around 0.88 (Fig. 7c). In uninfected cells, StIPP-GFP colocalized at the plasma membrane also with the PtdIns4P-biosensor mCherry<sub>FAPP1-PH</sub>, which also showed additional fluorescence in the nucleus (n) (Fig. 7d). Fluorescence intensities for StIPP-GFP and mCherry<sub>FAPP1-PH</sub> (Fig. 7e) recorded along the dashed line in Fig. 7(d), indicate a high degree of colocalization with a colocalization coefficient around 0.95 (Fig. 7f). The patterns for uninfected cells indicate that StIPP-GFP and biosensors for PtdIns(4,5)P<sub>2</sub> or PtdIns4P all colocalized at the plasma membrane.

Upon infection, both StIPP-GFP and mCherry<sub>PLC-PH</sub> decorated additional areas around the infection sites and the EHM (Fig. 7g) in a pattern consistent with recent reports on the accumulation of PtdIns(4,5)P<sub>2</sub> at pathogen infection sites in Arabidopsis (Shimada *et al.*, 2019; Qin *et al.*, 2020). StIPP-GFP and mCherry<sub>PLC-PH</sub> also associated with punctate structures in the vicinity of infection sites (arrows in Fig. 7g; Fig. S2). When the fluorescence intensities of StIPP-GFP and mCherry<sub>PLC-PH</sub> were quantified across the neck regions of penetrating *P. infestans* hyphae, a strong signal for StIPP-GFP was observed at the EHM, whereas the fluorescence intensity of mCherry<sub>PLC-PH</sub> was decreased in this area (Fig. 7g,h). The analysis of relative fluorescence intensities (Fig. 7h) across the infection structure (dashed line A in Fig. 7g) resulted in a negative Pearson coefficient for StIPP-GFP and mCherry<sub>PLC-PH</sub> (Fig. 7i), indicating a loss of the PtdIns(4,5)P<sub>2</sub>-biosensor fluorescence where StIPP-GFP intensity was high, which is consistent with StIPP-mediated hydrolysis of PtdIns(4,5)P<sub>2</sub>. By contrast, when the intensities for StIPP-GFP and mCherry<sub>PLC-PH</sub> were recorded across the plasma membrane of an infected cell (dashed line B in Fig. 7g), no inverted correlation was found (Fig. 7j,k) and the resulting pattern at the plasma membrane was similar to that observed in uninfected cells

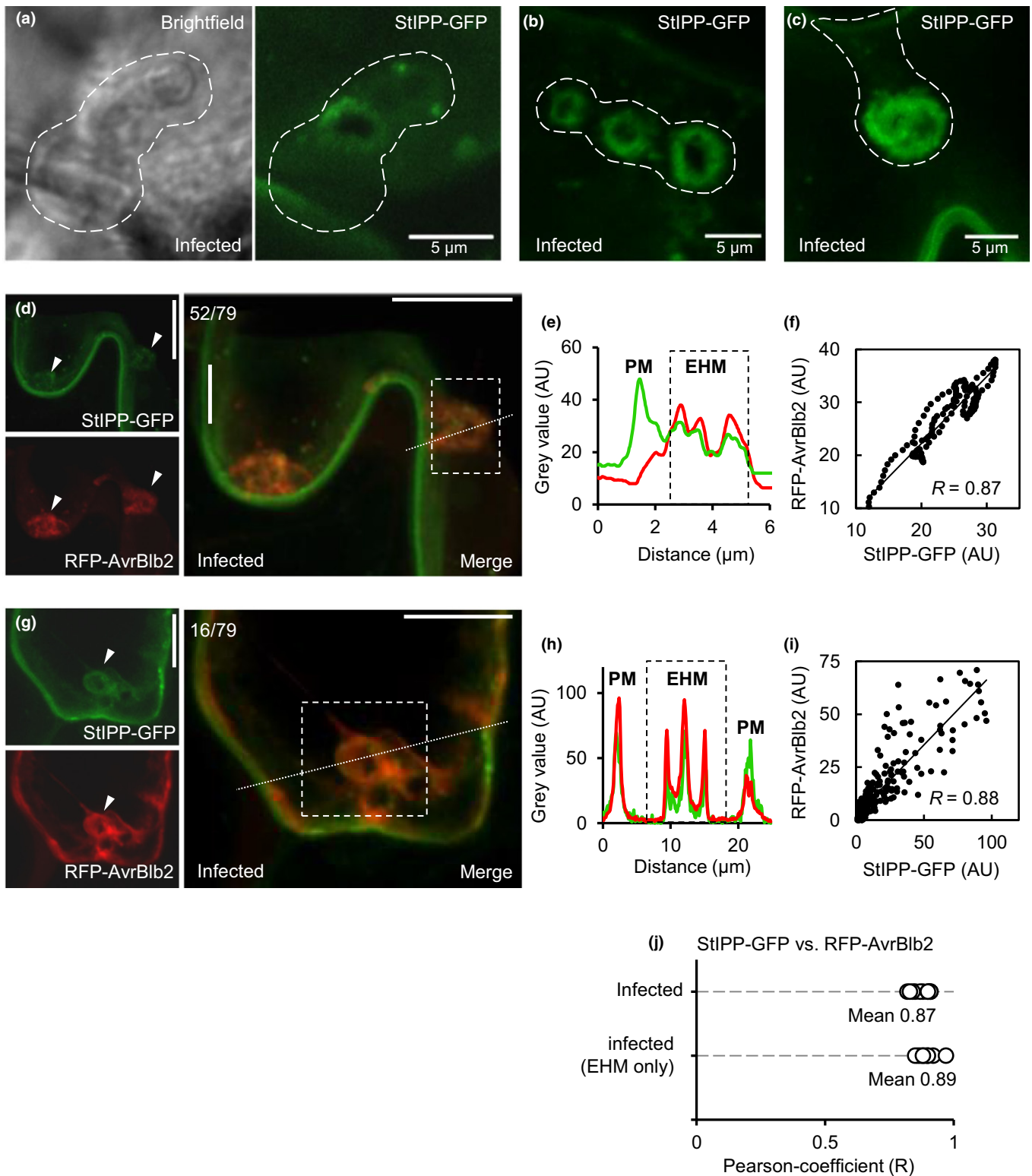


(Fig. 7a–c). The data suggest that conversion of  $\text{PtdIns}(4,5)\text{P}_2$  by StIPP might occur predominantly at the EHM.

When the subcellular distribution of  $\text{mCherry}_{\text{FAPP1-PH}}$  was analyzed relative to that of StIPP-GFP in infected cells, both StIPP-GFP and  $\text{mCherry}_{\text{FAPP1-PH}}$  displayed fluorescence at the

periphery of the neck region of penetrating hyphae (Fig. 7l), and the quantification of fluorescence intensities indicates close colocalization of StIPP-GFP and  $\text{mCherry}_{\text{FAPP1-PH}}$  in this area (Fig. 7m) with a high colocalization coefficient around 0.9 (Fig. 7n). StIPP-GFP and  $\text{mCherry}_{\text{FAPP1-PH}}$  also associated with

**Fig. 6** StIPP-GFP localizes to the extrahaustorial membrane (EHM) of tobacco epidermal cells infected with *Phytophthora infestans* 88069 ( $5 \times 10^4$  zoospores  $\text{ml}^{-1}$ ) in water 24 h after infiltration of agrobacteria. The subcellular localization of StIPP-GFP was analyzed in tobacco (*Nicotiana benthamiana*) epidermal cells upon infection with *P. infestans*. (a) Association of StIPP-GFP with infection sites. Left, bright field image; right, StIPP-GFP distribution. (b, c) Association of StIPP-GFP with extended regions of the EHM. Images in (a–c) are three-dimensional projections of confocal z-stacks and the outline of infection structures is indicated by dashed lines. (d–j) *Nicotiana benthamiana* leaves coexpressing StIPP-GFP and RFP-AvrBlb2 were infected with *P. infestans*. Images were recorded 3 d after inoculation. (d) Localization of StIPP-GFP with plasma membrane and with EHM (arrow heads), concomitant with RFP-AvrBlb2 only at the EHM. The white box indicates an infection structure with EHM. The dashed line indicates where intensity measurements were recorded. (e) Fluorescence intensity profiles recorded along the dashed line in (d), indicating colocalization of StIPP-GFP (green) with RFP-AvrBlb2 (red) at penetration sites. (f) Correlation analysis of the fluorescence intensities recorded for the EHM in (e) and corresponding Pearson coefficient. (g) Localization of StIPP-GFP and RFP-AvrBlb2 at plasma membrane and EHM (arrow heads). The white box indicates an infection structure with EHM. The dashed line indicates where intensity measurements were recorded. (h) Fluorescence intensity profiles recorded along the dashed line in (g), indicating colocalization of StIPP-GFP (green) with RFP-AvrBlb2 (red). (i) Correlation analysis of the fluorescence intensities recorded in (h) and corresponding Pearson coefficient. Numbers indicate the incidence of the observed localization patterns of StIPP-GFP. (j) Pearson coefficients for the colocalization of StIPP-GFP with RFP-AvrBlb2 were determined for 10 experiments, respectively, indicating a high degree of colocalization patterns for these markers, as indicated (0, no correlation; 1, perfect correlation). All markers were expressed under the control of the CaMV 35S promoter. AU, arbitrary units; EHM, extrahaustorial membrane; PM, plasma membrane; bars: (a–c) 5  $\mu\text{m}$ ; (d, g) 10  $\mu\text{m}$ . [Correction added after online publication 4 October 2020: panels (a) and (d) have been updated.]

punctate structures in the vicinity of infection sites (Fig. S2). Pearson coefficients for the colocalization of StIPP-GFP with the two lipid biosensors were determined for 10 experiments and indicate a high degree of colocalization of StIPP-GFP with the biosensors for PtdIns(4,5) $\text{P}_2$  and for PtdIns4P at the plasma membrane of uninfected and of infected cells (Fig. 7o). A notable exception is the inverse correlation (mean  $R = -0.62$ ) between high StIPP-GFP fluorescence and low intensity of the PtdIns(4,5) $\text{P}_2$  reporter mCherry<sub>PLC-PH</sub>, which was observed only at the EHM of infected cells (Fig. 7o), a pattern consistent with StIPP-mediated hydrolysis of PtdIns(4,5) $\text{P}_2$  predominantly at the EHM. Together, the data suggest StIPP-GFP action at *P. infestans* infection sites, which is accompanied by reduced intensity of a PtdIns(4,5) $\text{P}_2$ -specific biosensor.

### StIPP overexpression in Arabidopsis protoplasts leads to accumulation of FLS2

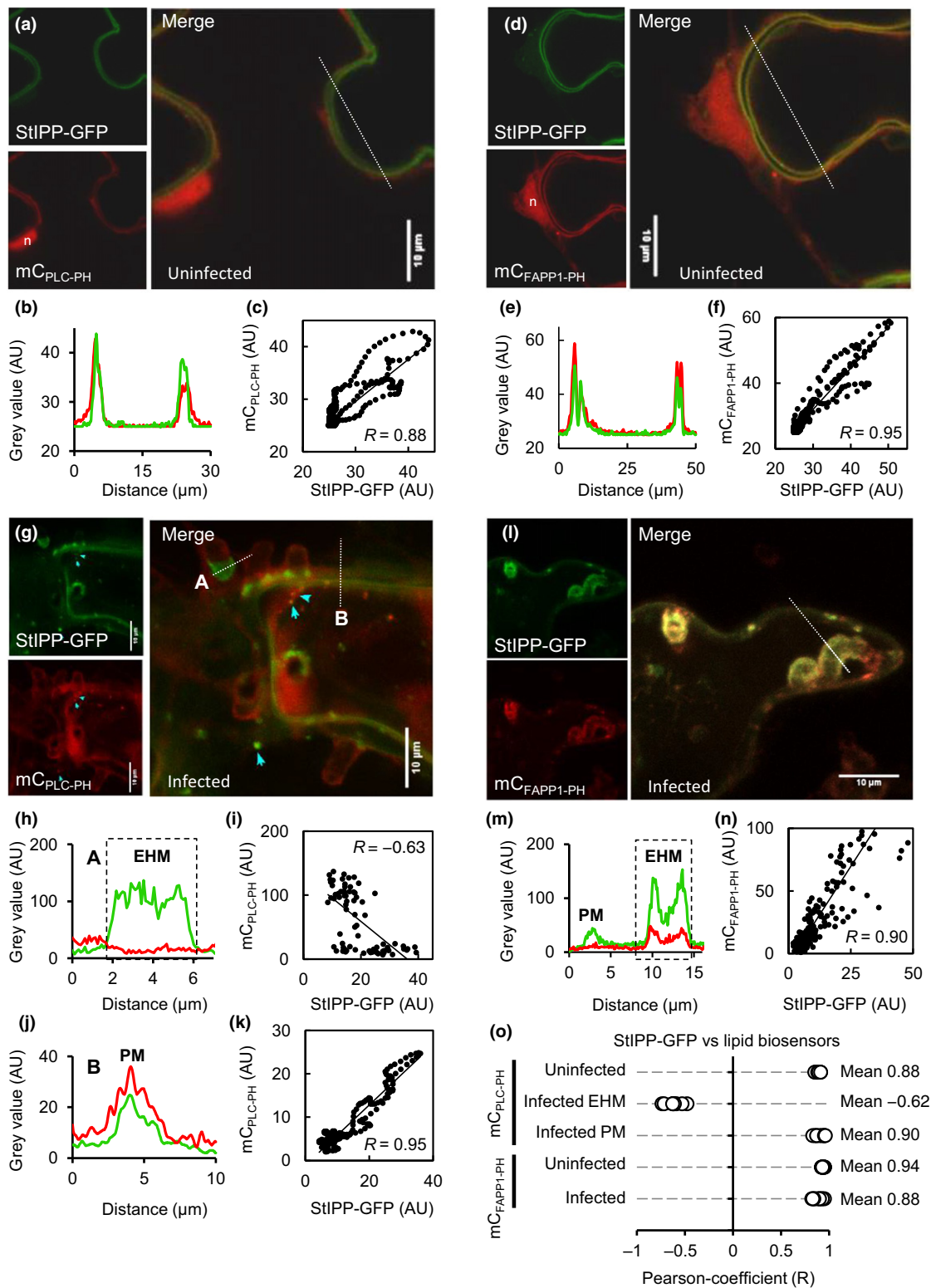
Experiments so far identified *StIPP* as a Pep-13-activated gene encoding a PtdIns(4,5) $\text{P}_2$ -specific 5-phosphatase, which may cause the dephosphorylation of PtdIns(4,5) $\text{P}_2$  at infection sites. As local interference with PtdIns(4,5) $\text{P}_2$  or enhanced formation of PtdIns4P may influence membrane trafficking, the abundance of membrane proteins with roles in defense might be altered upon StIPP action. To test this hypothesis, we analyzed the effects of StIPP-HA expression on the abundance of the receptor kinase FLS2 in Arabidopsis cells. Arabidopsis mesophyll protoplasts were transfected with *StIPP-HA* or *HA-CFP* expressed under the control of the CaMV 35S promoter. The abundance of intrinsic FLS2 protein was then analyzed 16 h post-transfection (hpt) by immunodetection using an FLS2-specific antibody (Fig. 8). The presence of the expressed proteins was verified by immunodetection using anti-HA antibodies (Fig. 8). FLS2 was detected at low levels in protoplasts expressing HA-CFP (Fig. 8a). By contrast, expression of StIPP-HA resulted in much stronger signals for FLS2 (Fig. 8a), indicating an increased abundance of the FLS2 protein. Increased abundance of FLS2 in cells expressing StIPP was also observed when FLS2 signals were quantified with a fluorescent western blot (Fig. 8b). In these experiments, mesophyll protoplasts were transfected as described earlier, FLS2

abundance was detected using a FLS2-specific antibody, and then a secondary antibody conjugated with a fluorescent dye was applied, and the fluorescence intensity of the dye was quantified. The data were normalized to the total loaded protein pre-labeled with the fluorescent dye (Fig. 8b). Analogous immunodetection experiments performed for PIN1, which does not accumulate at infection sites, did not indicate a significant change in PIN1 abundance (Fig. 8c). The combined observations indicate that modulation of PtdIns(4,5) $\text{P}_2$ /PtdIns4P levels by StIPP at infection sites (Fig. 7) might impact on the trafficking of defense-related membrane proteins, such as FLS2.

### Discussion

The molecular mechanisms underlying the defense of potato against the oomycete *P. infestans* are largely obscure. The present study provides evidence for an effect of Pep-13 treatment on the phosphoinositide-dependent modulation of vesicle trafficking, because (1) the Pep-13-activated potato gene, *StIPP*, encodes a functional PtdIns(4,5) $\text{P}_2$ -specific 5-phosphatase (Figs 3, 4); (2) StIPP-GFP relocates to *P. infestans* penetration sites upon infection (Fig. 6); and (3) StIPP-GFP influences the phosphoinositide system *in vivo* (Fig. 7), which controls membrane trafficking in plants and all other eukaryotes (Thole & Nielsen, 2008; Heilmann, 2016; Gerth *et al.*, 2017b).

PtdIns(4,5) $\text{P}_2$  accumulates in Arabidopsis plants at sites of pathogen infection (Shimada *et al.*, 2019; Qin *et al.*, 2020), and PtdIns(4,5) $\text{P}_2$  was identified as a susceptibility factor in Arabidopsis (Qin *et al.*, 2020). Therefore, the induction of StIPP, an enzyme hydrolyzing PtdIns(4,5) $\text{P}_2$  at the EHM, might be part of a defensive strategy of the host plant that involves limiting the availability of PtdIns(4,5) $\text{P}_2$  at infection sites. Our experiments provide evidence that in tobacco leaves PtdIns(4,5) $\text{P}_2$  correlates with *P. infestans* at infection sites (Fig. 7). While the association of PtdIns(4,5) $\text{P}_2$  with infection structures suggests a role in infection or defense processes, the precise molecular function of the lipid in this context is currently unclear. In our *in vitro* tests, StIPP activity was very specific and only converted PtdIns(4,5) $\text{P}_2$  to PtdIns4P, enabling a focused study of StIPP effects on cellular functions of these lipids.



PtdIns(4,5)P<sub>2</sub>, and possibly PtdIns4P, influence membrane trafficking by controlling both secretion and endocytosis. In pollen tubes the intricate balance of secretion and vesicle recycling is very sensitive to perturbation of cellular PtdIns(4,5)P<sub>2</sub> contents,

which results in aberrant deposition of pectin and morphological defects of the cells, such as tip branching and other characteristic shapes (Ischebeck *et al.*, 2008, 2011; Sousa *et al.*, 2008; Zhao *et al.*, 2010; Hempel *et al.*, 2017). When StlPP-YFP was

**Fig. 7** StIPP-GFP colocalizes with phosphoinositide biosensors at pathogen entry sites. The subcellular localization of StIPP-GFP was analyzed relative to the distribution of fluorescent probes for PtdIns(4,5)P<sub>2</sub> or for PtdIns4P upon transient expression in *Nicotiana benthamiana* leaves first without infection. (a–c) Coexpression of StIPP-GFP with mCherry<sub>PLC-PH</sub>, a fluorescent biosensor for PtdIns(4,5)P<sub>2</sub>, in uninfected leaves. (a) Fluorescence images indicating plasma membrane association of StIPP-GFP and of mCherry<sub>PLC-PH</sub>. n, nucleus. (b) Fluorescence intensity profiles recorded along the dashed line in (a), indicating colocalization of StIPP-GFP (green) with mCherry<sub>PLC-PH</sub> (red). (c) Correlation analysis of the fluorescence intensities recorded in (b) and corresponding Pearson coefficient. (d–f) Coexpression of StIPP-GFP with mCherry<sub>FAPP1-PH</sub>, a fluorescent biosensor for PtdIns4P in uninfected leaves. (d) Fluorescence images indicating plasma membrane association of StIPP-GFP and of mCherry<sub>FAPP1-PH</sub>. n, nucleus. (e) Fluorescence intensity profiles recorded along the dashed line in (d), indicating colocalization of StIPP-GFP (green) with mCherry<sub>FAPP1-PH</sub> (red). (f) Correlation analysis of the fluorescence intensities recorded in (e) and corresponding Pearson coefficient. Further experiments were performed to monitor the distribution of StIPP-GFP relative to that of phosphoinositide biosensors upon infection with *Phytophthora infestans* 24 h after infiltration of agrobacteria. (g–k) Coexpression of StIPP-GFP with mCherry<sub>PLC-PH</sub> in infected leaves. (g) Fluorescence images indicating association of StIPP-GFP and of mCherry<sub>PLC-PH</sub> with the extrahaustorial membrane (EHM) of infection sites. Blue arrows highlight punctate signals. (h) Fluorescence intensity profiles recorded along the dashed line A in (g), indicating an inverted intensity correlation of StIPP-GFP (green) with mCherry<sub>PLC-PH</sub> (red) at the EHM. (i) Correlation analysis of the fluorescence intensities recorded in (h) and corresponding negative Pearson coefficient. (j) Fluorescence intensity profiles recorded along the dashed line B in (g), indicating colocalization of StIPP-GFP (green) with mCherry<sub>PLC-PH</sub> (red) at the plasma membrane of infected cells. (k) Correlation analysis of the fluorescence intensities recorded in (j) and corresponding positive Pearson coefficient. (l–n) Coexpression of StIPP-GFP with mCherry<sub>FAPP1-PH</sub> in infected leaves. (l) Fluorescence images indicating association of StIPP-GFP and of mCherry<sub>FAPP1-PH</sub> with the EHM of infection sites. (m) Fluorescence intensity profiles recorded along the dashed line in (l), indicating colocalization of StIPP-GFP (green) with mCherry<sub>PLC-PH</sub> (red) at the EHM. (n) Correlation analysis of the fluorescence intensities recorded in (m) and corresponding Pearson coefficient. (o) Pearson coefficients for the colocalization of StIPP-GFP with the phosphoinositide biosensors were determined for 10 experiments, respectively, with experimental parameters as indicated. A negative correlation was observed for the intensities of StIPP-GFP and mCherry<sub>PLC-PH</sub> at the EHM of infected cells (< 0, inverted correlation; 0, no correlation; 1, perfect correlation). All markers were expressed under the control of the CaMV 35S promoter. AU, arbitrary units; EHM, extrahaustorial membrane; PM, plasma membrane; bars, 10 μm.

expressed in pollen, pollen tube germination from the grains was often aborted (Fig. 4d), consistent with defects observed in *Arabidopsis pip5k4 pip5k5* double mutants deficient in PtdIns(4,5)P<sub>2</sub> formation (Ischebeck *et al.*, 2008; Sousa *et al.*, 2008). Furthermore, StIPP-YFP expression antagonized the enhanced pollen tube tip branching and stunted tube growth caused by PIP5K5-mediated overproduction of PtdIns(4,5)P<sub>2</sub> (Fig. 4e–g), consistent with PtdIns(4,5)P<sub>2</sub> dephosphorylation and a functional effect on membrane trafficking much like that of other PtdIns(4,5)P<sub>2</sub>-specific 5-phosphatases, such as AtPTase11 (Ercetin *et al.*, 2008) or Sac9 (Williams *et al.*, 2005). While the results from the pollen tube model may at first appear unrelated to a role of StIPP in defense, it has recently been shown that PtdIns(4,5)P<sub>2</sub> production at the apical plasma membrane of pollen tubes is controlled by phosphorylation of PI4P 5-kinases by the MAP-kinase MPK6 (Hempel *et al.*, 2017). Importantly, MPK6 also has a demonstrated role in PAMP-responses and pathogen defense (Meng & Zhang, 2013), and a PAMP-triggered MAPK-cascade involving MPK6 has recently been shown to inhibit the formation of PtdIns(4,5)P<sub>2</sub> in *Arabidopsis* (Menzel *et al.*, 2019). Evidently, the limitation of cellular PtdIns(4,5)P<sub>2</sub> by means of inhibiting its biosynthesis might be part of the plant defensive strategy against pathogen attack. Our data from the potato/*P. infestans* model provide further evidence for this concept, with the noted difference that here PtdIns(4,5)P<sub>2</sub> is reduced by enhancing its breakdown through the activation of StIPP.

In infected tobacco epidermal cells, StIPP relocated from general plasma membrane association (as also observed in pollen tubes) to sites of *P. infestans* penetration (Fig. 6). The specific recruitment to infection sites suggests a change in protein–protein or protein–lipid interactions of StIPP that is mediated by the infection. Importantly, the imaging data also provide evidence for StIPP-mediated localized hydrolysis of PtdIns(4,5)P<sub>2</sub> (Fig. 7g–k) and for the concomitant formation of PtdIns4P

(Fig. 7l–n), suggesting that StIPP locally inhibits PtdIns(4,5)P<sub>2</sub>-dependent processes. The quantitative *in vivo* imaging of processes at dynamic infection structures represents a substantial experimental challenge. Therefore, the results from our imaging approach should not be overinterpreted. Negative Pearson coefficients for the relative localizations of StIPP-GFP and mCherry<sub>PLC-PH</sub> were only observed at the EHM of infected cells, whereas in other subcellular locations the respective Pearson coefficients were positive, regardless of whether cells were infected or not. Taking these data at face-value, this pattern suggests that conversion of PtdIns(4,5)P<sub>2</sub> by StIPP occurred predominantly at the EHM. A possible conclusion is that StIPP might require a post-translational activation step at the EHM in addition to the induction of its transcript and its relocation from the plasma membrane to the EHM. Our observation of a significant accumulation of the immune receptor FLS2 upon StIPP expression in *Arabidopsis* protoplasts (Fig. 8) supports the hypothesis that reduced PtdIns(4,5)P<sub>2</sub> results in attenuated rates of clathrin-mediated endocytosis (CME). As PtdIns(4,5)P<sub>2</sub> is a key mediator of CME (König *et al.*, 2008b; Zhao *et al.*, 2010; Ischebeck *et al.*, 2013; Tejos *et al.*, 2014; Menzel *et al.*, 2019), the observed accumulation of FLS2 (Fig. 8) may reflect modulated endocytosis, which results in the stabilization of the receptor at the plasma membrane. Future studies will show whether StIPP regulates vesicular trafficking of specific membrane proteins during the immune response.

It is possible that the activation of StIPP and its recruitment to sites of infection is part of a mechanism to locally and transiently stabilize plasma membrane proteins with roles in immunity only where an infection actually occurs. As plant defense responses are highly complex, it is clear that StIPP will only be one element in the multi-layered series of events. In line with this notion, we did not observe altered susceptibility or resistance against *P. infestans* in transgenic potato plants expressing RNAi constructs against

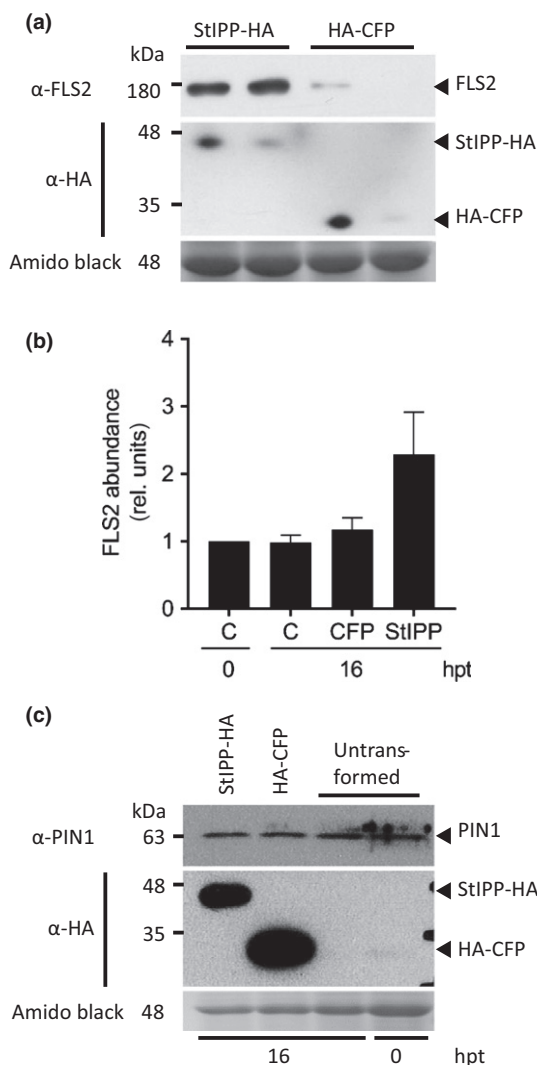


**Fig. 8** StIPP overexpression in Arabidopsis protoplasts leads to stabilization of FLS2. The effects of StIPP expression on the abundance of the plasma membrane protein FLS2 was tested in Arabidopsis mesophyll protoplasts transformed with StIPP-HA or HA-CFP under the control of the CaMV 35S promoter. (a) Samples were harvested 16 h post-transfection (hpt) and subjected to western blot analysis using anti-FLS2 or anti-HA antibodies. Membranes were stained with amido black to verify equal loading of protein extracts. Arrowheads indicate the migration of detected proteins, as indicated. The molecular weight marker is shown on the left. The blot shown is representative for five out of six experiments. (b) Quantification of FLS2 abundance in Arabidopsis protoplasts 16 hpt. Controls (C) were performed using untransformed protoplasts harvested directly after transfection (0) or together with HA-CFP and StIPP-HA expressing protoplasts, as indicated. The data represent mean  $\pm$  standard deviation from three quantitative fluorescent western blot experiments. (c) PIN1 abundance is not altered in StIPP expressing protoplasts. StIPP-HA and HA-CFP fusion constructs were transiently expressed in Arabidopsis Col-0 protoplasts under the control of the 35S promoter. Total protein was extracted 0 and 16 h after transformation and subjected to western blot analysis using  $\alpha$ -PIN1 antibodies and  $\alpha$ -HA-antibodies. The membrane was stained with amido black to visualize loading. Arrowheads indicate the migration of detected proteins, as indicated. The molecular weight marker is shown on the left. The blot shown is representative for five out of five experiments.

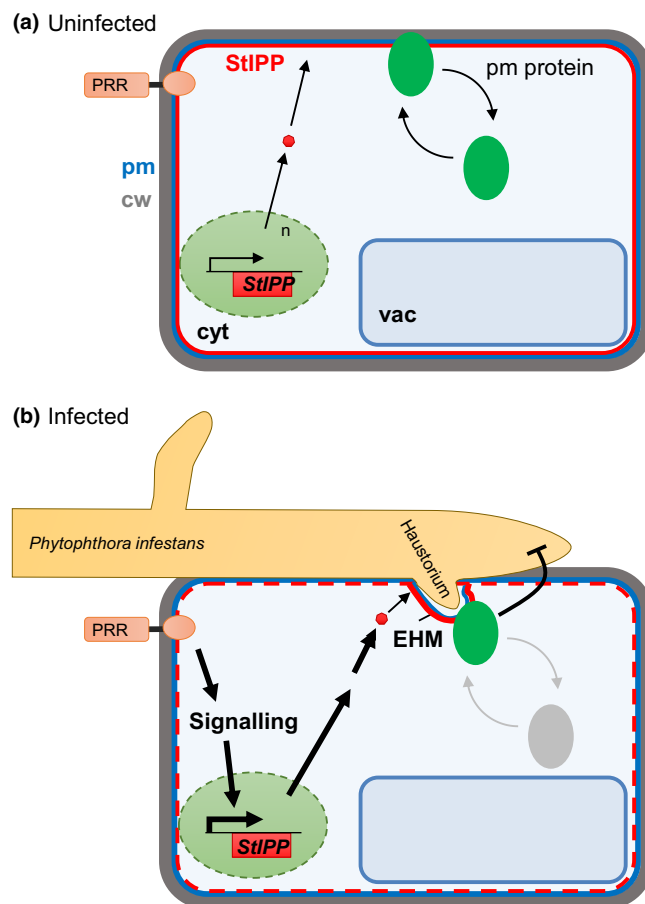


**Fig. 9** A model for the role of StIPP in pathogen defense. In uninfected cells (a), there is little or no expression of the StIPP gene. Any StIPP protein might associate with the plasma membrane. Upon PAMP-treatment or pathogen attack (b), the expression of StIPP is activated, resulting in the association of the enzyme with the plasma membrane, concentrated around the sites of penetration. As a PtdIns(4,5) $P_2$ -specific 5-phosphatase, StIPP may attenuate PtdIns(4,5) $P_2$ -dependent recycling of plasma membrane-resident proteins, possibly resulting in reduced recycling, indicated by the gray oval, and their transient stabilization at the plasma membrane. Other explanations are possible. Thicker arrows indicate an enhanced effect. cw, cell wall; cyt, cytosol; EHM, extra-haustorial membrane; n, nucleus; pm, plasma membrane; PRR, pattern recognition receptor; red circle, StIPP; vac, vacuole.

StIPP, despite substantial downregulation of StIPP transcript abundance in these plants (Fig. S3). Nonetheless, our data suggest that the StIPP protein contributes to defense, likely through its localized effects on the phosphoinositide system and vesicle trafficking at infection sites. As illustrated in the model shown in Fig. 9, StIPP may, thus, be part of transient reprogramming of membrane trafficking processes at the plasma membrane, which concentrates at the perceived sites of *P. infestans* infection.

## Acknowledgements

The authors thank Dr Jennifer Lerche, Dr Tobias Heinz and Dr Mareike Heilmann (all at the Department for Cellular Biochemistry, Institute of Biochemistry and Biotechnology, Martin-Luther-University Halle-Wittenberg, Germany) for technical

support and helpful discussion. Dr Yasin Dagdas and Dr Sophien Kamoun (The Sainsbury Laboratory, Norwich, UK) are acknowledged for kindly providing AvrB1b2 and the *P. infestans* isolate 88069, respectively. Financial support by the German Research Foundation (DFG) is gratefully acknowledged (grants CRC648 TP A4 to SR and He3424/1-1, CRC648 TP B10, CRC648 TP B13 and INST271/371-1 FUGG to IH).

## Author contributions

JR, IS, RS, MF and MT performed experiments, JR, IS, MT, SR and IH designed research, JR, IS and MT commented on the manuscript, SR and IH wrote the manuscript.

## ORCID

Marta Fratini  <https://orcid.org/0000-0003-0934-3854>  
Ingo Heilmann  <https://orcid.org/0000-0002-2324-1849>  
Sabine Rosahl  <https://orcid.org/0000-0002-7300-5596>  
Marco Trujillo  <https://orcid.org/0000-0002-5470-7277>

## References

- Aibara I, Miwa K. 2014. Strategies for optimization of mineral nutrient transport in plants: multilevel regulation of nutrient-dependent dynamics of root architecture and transporter activity. *Plant and Cell Physiology* 55: 2027–2036.
- Ben Khaled S, Postma J, Robatzek S. 2015. A moving view: subcellular trafficking processes in pattern recognition receptor-triggered plant immunity. *Annual review of Phytopathology* 53: 379–402.
- Berdy SE, Kudla J, Gruissem W, Gillaspay GE. 2001. Molecular characterization of At5PTase1, an inositol phosphatase capable of terminating inositol trisphosphate signaling. *Plant Physiology* 126: 801–810.
- Bozkurt TO, Belhaj K, Dagdas YF, Chaparro-Garcia A, Wu CH, Cano LM, Kamoun S. 2015. Rerouting of plant late endocytic trafficking toward a pathogen interface. *Traffic* 16: 204–226.
- Bozkurt TO, Richardson A, Dagdas YF, Mongrand S, Kamoun S, Raffaele S. 2014. The plant membrane-associated REMORIN1.3 accumulates in discrete perihair domains and enhances susceptibility to *Phytophthora infestans*. *Plant Physiology* 165: 1005–1018.
- Bozkurt TO, Schornack S, Win J, Shindo T, Ilyas M, Oliva R, Cano LM, Jones AM, Huitema E, van der Hoorn RA *et al.* 2011. *Phytophthora infestans* effector AVRblb2 prevents secretion of a plant immune protease at the haustorial interface. *Proceedings of the National Academy of Sciences, USA* 108: 20832–20837.
- Brunner F, Rosahl S, Lee J, Rudd JJ, Geiler C, Kauppinen S, Rasmussen G, Scheel D, Nürnberger T. 2002. Pep-13, a plant defense-inducing pathogen-associated pattern from *Phytophthora* transglutaminases. *EMBO Journal* 21: 6681–6688.
- Chinchilla D, Bauer Z, Regenass M, Boller T, Felix G. 2006. The *Arabidopsis* receptor kinase FLS2 binds flg22 and determines the specificity of flagellin perception. *Plant Cell* 18: 465–476.
- Cho MH, Chen Q, Okpodu CM, Boss WF. 1992. Separation and quantification of [<sup>3</sup>H]inositol phospholipids using thin-layer-chromatography and a computerized <sup>3</sup>H imaging scanner. *LC-GC* 10: 464–468.
- Chomczynski P, Sacchi N. 1987. Single-step method of RNA isolation by acid guanidinium thiocyanate-phenol-chloroform extraction. *Analytical Biochemistry* 162: 156–159.
- Cohen YR. 2002. Beta-aminobutyric acid-induced resistance against plant pathogens. *Plant Disease* 86: 448–457.
- Collins NC, Thordal-Christensen H, Lipka V, Bau S, Kombrink E, Qiu JL, Huckelhoven R, Stein M, Freialdenhoven A, Somerville SC *et al.* 2003. SNARE-protein-mediated disease resistance at the plant cell wall. *Nature* 425: 973–977.
- Dobritzsch M, Lubken T, Eschen-Lippold L, Gorzalka K, Blum E, Matern A, Marillonnet S, Bottcher C, Dräger B, Rosahl S. 2016. MATE transporter-dependent export of hydroxycinnamic acid amides. *Plant Cell* 28: 583–596.
- Dyson MR, Shadbolt SP, Vincent KJ, Perera RL, McCafferty J. 2004. Production of soluble mammalian proteins in *Escherichia coli*: identification of protein features that correlate with successful expression. *BMC Biotechnology* 4: 32.
- Ercetin ME, Ananieva EA, Safaei NM, Torabinejad J, Robinson JY, Gillaspay GE. 2008. A phosphatidylinositol phosphate-specific myo-inositol polyphosphate 5-phosphatase required for seedling growth. *Plant Molecular Biology* 67: 375–388.
- Ercetin ME, Gillaspay GE. 2004. Molecular characterization of an *Arabidopsis* gene encoding a phospholipid-specific inositol polyphosphate 5-phosphatase. *Plant Physiology* 135: 938–946.
- Eschen-Lippold L, Altmann S, Rosahl S. 2010. DL-beta-Aminobutyric acid-induced resistance of potato against *Phytophthora infestans* requires salicylic acid but not oxylipins. *Molecular Plant-Microbe Interactions* 23: 585–592.
- Eschen-Lippold L, Landgraf R, Smolka U, Schulze S, Heilmann M, Heilmann I, Hause G, Rosahl S. 2012. Activation of defense against *Phytophthora infestans* in potato by down-regulation of syntaxin gene expression. *New Phytologist* 193: 985–996.
- Felsenstein J. 1985. Confidence limits on phylogenies: an approach using the bootstrap. *Evolution* 39: 783–791.
- Fry W. 2008. *Phytophthora infestans*: the plant (and R gene) destroyer. *Molecular Plant Pathology* 9: 385–402.
- Gerth K, Lin F, Daamen F, Menzel W, Heinrich F, Heilmann M. 2017a. *Arabidopsis* phosphatidylinositol 4-phosphate 5-kinase 2 contains a functional nuclear localization sequence and interacts with alpha-importins. *The Plant Journal* 92: 862–878.
- Gerth K, Lin F, Menzel W, Krishnamoorthy P, Stenzel I, Heilmann M, Heilmann I. 2017b. Guilt by association: a phenotype-based view of the plant phosphoinositide network. *Annual Review of Plant Biology* 68: 349–374.
- Gillaspay GE. 2013. The role of phosphoinositides and inositol phosphates in plant cell signaling. *Advances in Experimental Medicine and Biology* 991: 141–157.
- Golani Y, Kaye Y, Gilhar O, Ercetin M, Gillaspay G, Levine A. 2013. Inositol polyphosphate phosphatidylinositol 5-phosphatase9 (At5ptase9) controls plant salt tolerance by regulating endocytosis. *Molecular Plant* 6: 1781–1794.
- Gunesequera B, Torabinejad J, Robinson J, Gillaspay GE. 2007. Inositol polyphosphate 5-phosphatases 1 and 2 are required for regulating seedling growth. *Plant Physiology* 143: 1408–1417.
- Halim VA, Altmann S, Ellinger D, Eschen-Lippold L, Miersch O, Scheel D, Rosahl S. 2009. PAMP-induced defense responses in potato require both salicylic acid and jasmonic acid. *The Plant Journal* 57: 230–242.
- Halim VA, Hunger A, Macioszek V, Landgraf P, Nürnberger T, Scheel D, Rosahl S. 2004. The oligopeptide elicitor Pep-13 induces salicylic acid-dependent and-independent defense reactions in potato. *Physiological and Molecular Plant Pathology* 64: 311–318.
- Heilmann I. 2016. Phosphoinositide signaling in plant development. *Development* 143: 2044–2055.
- Helling D, Possart A, Cottier S, Klahre U, Kost B. 2006. Pollen tube tip growth depends on plasma membrane polarization mediated by tobacco PLC3 activity and endocytic membrane recycling. *Plant Cell* 18: 3519–3534.
- Hempel F, Stenzel I, Heilmann M, Krishnamoorthy P, Menzel W, Golbik R, Helm S, Dobritzsch D, Baginsky S, Lee J *et al.* 2017. MAPKs influence pollen tube growth by controlling the formation of phosphatidylinositol 4,5-bisphosphate in an apical plasma membrane domain. *Plant Cell* 29: 3030–3050.
- Hung CY, Aspesi P Jr, Hunter MR, Lomax AW, Perera IY. 2014. Phosphoinositide-signaling is one component of a robust plant defense response. *Frontiers in Plant Science* 5: 267.
- Ischebeck T, Stenzel I, Heilmann I. 2008. Type B phosphatidylinositol-4-phosphate 5-kinases mediate pollen tube growth in *Nicotiana tabacum* and *Arabidopsis* by regulating apical pectin secretion. *Plant Cell* 20: 3312–3330.
- Ischebeck T, Stenzel I, Hempel F, Jin X, Mosblech A, Heilmann I. 2011. Phosphatidylinositol-4,5-bisphosphate influences Nt-Rac5-mediated cell

- expansion in pollen tubes of *Nicotiana tabacum*. *The Plant Journal* 65: 453–468.
- Ischebeck T, Vu LH, Jin X, Stenzel I, Löffke C, Heilmann I. 2010. Functional cooperativity of enzymes of phosphoinositide conversion according to synergistic effects on pectin secretion in tobacco pollen tubes. *Molecular Plant* 3: 870–881.
- Ischebeck T, Werner S, Krishnamoorthy P, Lerche J, Meijon M, Stenzel I, Löffke C, Wiessner T, Im YJ, Perera IY *et al.* 2013. Phosphatidylinositol 4,5-bisphosphate influences PIN polarization by controlling clathrin-mediated membrane trafficking in *Arabidopsis*. *Plant Cell* 25: 4894–4911.
- Johanson U, Karlsson M, Johansson I, Gustavsson S, Sjövall S, Frayse L, Weig AR, Kjellbom P. 2001. The complete set of genes encoding major intrinsic proteins in *Arabidopsis* provides a framework for a new nomenclature for major intrinsic proteins in plants. *Plant Physiology* 126: 1358–1369.
- Kadota Y, Sklenar J, Derbyshire P, Stransfeld L, Asai S, Ntoukakis V, Jones JD, Shirasu K, Menke F, Jones A *et al.* 2014. Direct regulation of the NADPH oxidase RBOHD by the PRR-associated kinase BIK1 during plant immunity. *Molecular Cell* 54: 43–55.
- Karimi M, Inze D, Depicker A. 2002. GATEWAY vectors for *Agrobacterium*-mediated plant transformation. *Trends in Plant Science* 7: 193–195.
- Kloosterman B, De Koeijer D, Griffiths R, Flinn B, Steuernagel B, Scholz U, Sonnewald S, Sonnewald U, Bryan GJ, Prat S *et al.* 2008. Genes driving potato tuber initiation and growth: identification based on transcriptional changes using the POCI array. *Functional & Integrative Genomics* 8: 329–340.
- König S, Hoffmann M, Mosblech A, Heilmann I. 2008a. Determination of content and fatty acid composition of unlabeled phosphoinositide species by thin layer chromatography and gas chromatography. *Analytical Biochemistry* 378: 197–201.
- König S, Ischebeck T, Lerche J, Stenzel I, Heilmann I. 2008b. Salt stress-induced association of phosphatidylinositol-4,5-bisphosphate with clathrin-coated vesicles in plants. *Biochemical Journal* 415: 387–399.
- Kusano H, Testerink C, Vermeer JEM, Tsuge T, Shimada H, Oka A, Munnik T, Aoyama T. 2008. The *Arabidopsis* phosphatidylinositol phosphate 5-kinase PIP5K3 is a key regulator of root hair tip growth. *Plant Cell* 20: 367–380.
- Landgraf R, Smolka U, Altmann S, Eschen-Lippold L, Senning M, Sonnewald S, Weigel B, Frolova N, Strehmel N, Hause G *et al.* 2014. The ABC transporter ABCG1 is required for suberin formation in potato tuber periderm. *Plant Cell* 26: 3403–3415.
- van Leeuwen W, Vermeer JE, Gadella TW Jr, Munnik T. 2007. Visualization of phosphatidylinositol 4,5-bisphosphate in the plasma membrane of suspension-cultured tobacco BY-2 cells and whole *Arabidopsis* seedlings. *The Plant Journal* 52: 1014–1026.
- Lipka V, Kwon C, Panstruga R. 2007. SNARE-ware: the role of SNARE-domain proteins in plant biology. *Annual Review of Cell and Developmental Biology* 23: 147–174.
- Majerus PW, York JD. 2009. Phosphoinositide phosphatases and disease. *Journal of Lipid Research* 50: S249–254.
- Mei Y, Jia WJ, Chu YJ, Xue HW. 2012. *Arabidopsis* phosphatidylinositol monophosphate 5-kinase 2 is involved in root gravitropism through regulation of polar auxin transport by affecting the cycling of PIN proteins. *Cell Research* 22: 581–597.
- Meng X, Zhang S. 2013. MAPK cascades in plant disease resistance signaling. *Annual Review of Phytopathology* 51: 245–266.
- Menzel W, Stenzel I, Helbig LM, Krishnamoorthy P, Neumann S, Eschen-Lippold L, Heilmann M, Lee J, Heilmann I. 2019. A PAMP-triggered MAPK cascade inhibits phosphatidylinositol 4,5-bisphosphate production by PIP5K6 in *Arabidopsis thaliana*. *New Phytologist* 224: 833–847.
- Mishkind M, Vermeer JE, Darwish E, Munnik T. 2009. Heat stress activates phospholipase D and triggers PIP accumulation at the plasma membrane and nucleus. *The Plant Journal* 60: 10–21.
- Nakagawa T, Kurose T, Hino T, Tanaka K, Kawamukai M, Niwa Y, Toyooka K, Matsuoka K, Jinbo T, Kimura T. 2007. Development of series of gateway binary vectors, pGWBs, for realizing efficient construction of fusion genes for plant transformation. *Journal of Bioscience and Bioengineering* 104: 34–41.
- Qin L, Zhou Z, Li Q, Zhai C, Liu L, Quilichini TD, Gao P, Kessler SA, Jaillais Y, Datla R *et al.* 2020. Specific recruitment of phosphoinositide species to the plant-pathogen interfacial membrane underlies *Arabidopsis* susceptibility to fungal infection. *Plant Cell* 32: 1665–1688.
- Robatzek S, Chinchilla D, Boller T. 2006. Ligand-induced endocytosis of the pattern recognition receptor FLS2 in *Arabidopsis*. *Genes & Development* 20: 537–542.
- Saeed B, Brillada C, Trujillo M. 2019. Dissecting the plant exocyst. *Current Opinion in Plant Biology* 52: 69–76.
- Saitou N, Nei M. 1987. The neighbor-joining method: a new method for reconstructing phylogenetic trees. *Molecular Biology and Evolution* 4: 406–425.
- Schulze-Lefert P. 2004. Knocking on the heaven's wall: pathogenesis of and resistance to biotrophic fungi at the cell wall. *Current Opinion in Plant Biology* 7: 377–383.
- Shimada TL, Betsuyaku S, Inada N, Ebine K, Fujimoto M, Uemura T, Takano Y, Fukuda H, Nakano A, Ueda T. 2019. Enrichment of phosphatidylinositol 4,5-bisphosphate in the extra-invasive hyphal membrane promotes colletotrichum infection of *Arabidopsis thaliana*. *Plant and Cell Physiology* 60: 1514–1524.
- Si-Ammour A, Mauch-Mani B, Mauch F. 2003. Quantification of induced resistance against *Phytophthora* species expressing GFP as a vital marker: beta-aminobutyric acid but not BTH protects potato and *Arabidopsis* from infection. *Molecular Plant Pathology* 4: 237–248.
- Simon ML, Platre MP, Assil S, van Wijk R, Chen WY, Chory J, Dreux M, Munnik T, Jaillais Y. 2014. A multi-colour/multi-affinity marker set to visualize phosphoinositide dynamics in *Arabidopsis*. *The Plant Journal* 77: 322–337.
- Sousa E, Kost B, Malho R. 2008. *Arabidopsis* phosphatidylinositol-4-monophosphate 5-kinase 4 regulates pollen tube growth and polarity by modulating membrane recycling. *Plant Cell* 20: 3050–3064.
- Stenzel I, Ischebeck T, König S, Holubowska A, Sporysz M, Hause B, Heilmann I. 2008. The type B phosphatidylinositol-4-phosphate 5-kinase 3 is essential for root hair formation in *Arabidopsis thaliana*. *Plant Cell* 20: 124–141.
- Stenzel I, Ischebeck T, Quint M, Heilmann I. 2012. Variable regions of PI4P 5-kinases direct PtdIns(4,5)P<sub>2</sub> toward alternative regulatory functions in tobacco pollen tubes. *Frontiers in Plant Science* 2: 1–14.
- Stenzel I, Ischebeck T, Vu-Becker LH, Riechmann M, Krishnamoorthy P, Fratini M, Heilmann I. 2020. Coordinated localization and antagonistic function of NtPLC3 and PI4P 5-kinases in the subapical plasma membrane of tobacco pollen tubes. *Plants (Basel)* 9: 452.
- Stevenson-Paulik J, Bastidas RJ, Chiou ST, Frye RA, York JD. 2005. Generation of phytate-free seeds in *Arabidopsis* through disruption of inositol polyphosphate kinases. *Proceedings of the National Academy of Sciences, USA* 102: 12612–12617.
- Tamura K, Peterson D, Peterson N, Stecher G, Nei M, Kumar S. 2011. MEGA5: molecular evolutionary genetics analysis using maximum likelihood, evolutionary distance, and maximum parsimony methods. *Molecular Biology and Evolution* 28: 2731–2739.
- Tejos R, Sauer M, Vanneste S, Palacios-Gomez M, Li H, Heilmann M, van Wijk R, Vermeer JE, Heilmann I, Munnik T *et al.* 2014. Bipolar plasma membrane distribution of phosphoinositides and their requirement for auxin-mediated cell polarity and patterning in *Arabidopsis*. *Plant Cell* 26: 2114–2128.
- Thole JM, Nielsen E. 2008. Phosphoinositides in plants: novel functions in membrane trafficking. *Current Opinion in Plant Biology* 11: 620–631.
- Vincent P, Chua M, Nogue F, Fairbrother A, Mekeel H, Xu Y, Allen N, Bibikova TN, Gilroy S, Bankaitis VA. 2005. A Sec14p-nodulin domain phosphatidylinositol transfer protein polarizes membrane thaliana root hairs. *Journal of Cell Biology* 168: 801–812.
- Wang W, Liu N, Gao C, Cai H, Romeis T, Tang D. 2020. The *Arabidopsis* exocyst subunits EXO70B1 and EXO70B2 regulate FLS2 homeostasis at the plasma membrane. *New Phytologist* 227: 529–544.
- Wesley SV, Helliwell CA, Smith NA, Wang MB, Rouse DT, Liu Q, Gooding PS, Singh SP, Abbott D, Stoutjesdijk PA *et al.* 2001. Construct design for efficient, effective and high-throughput gene silencing in plants. *The Plant Journal* 27: 581–590.
- Williams ME, Torabinejad J, Cohick E, Parker K, Drake EJ, Thompson JE, Hortter M, Dewald DB. 2005. Mutations in the *Arabidopsis* phosphoinositide phosphatase gene *SAC9* lead to overaccumulation of PtdIns(4,5)P<sub>2</sub> and

- constitutive expression of the stress-response pathway. *Plant Physiology* 138: 686–700.
- Yoo SD, Cho YH, Sheen J. 2007. *Arabidopsis* mesophyll protoplasts: a versatile cell system for transient gene expression analysis. *Nature Protocols* 2: 1565–1572.
- Zhao Y, Yan A, Feijo JA, Furutani M, Takenawa T, Hwang I, Fu Y, Yang Z. 2010. Phosphoinositides regulate clathrin-dependent endocytosis at the tip of pollen tubes in *Arabidopsis* and tobacco. *Plant Cell* 22: 4031–4044.
- Zuckerkindl E, Pauling L. 1965. Evolutionary divergence and convergence of proteins. In: Bryson V, Vogel HJ, eds. *Evolving genes and proteins*. New York, NY, USA: Academic Press, 97–166.

## Supporting Information

Additional Supporting Information may be found online in the Supporting Information section at the end of the article.

**Fig. S1** Soluble inositol phosphates are not converted by recombinant StIPP *in vitro*.

**Fig. S2** Association of phosphoinositide biosensors with punctate patterns around *Phytophthora infestans* infection sites.

**Fig. S3** *Phytophthora infestans* growth is not altered on transgenic StIPP-RNAi plants.

Please note: Wiley Blackwell are not responsible for the content or functionality of any Supporting Information supplied by the authors. Any queries (other than missing material) should be directed to the *New Phytologist* Central Office.



## About New Phytologist

- *New Phytologist* is an electronic (online-only) journal owned by the New Phytologist Foundation, a **not-for-profit organization** dedicated to the promotion of plant science, facilitating projects from symposia to free access for our Tansley reviews and Tansley insights.
- Regular papers, Letters, Research reviews, Rapid reports and both Modelling/Theory and Methods papers are encouraged. We are committed to rapid processing, from online submission through to publication 'as ready' via *Early View* – our average time to decision is <26 days. There are **no page or colour charges** and a PDF version will be provided for each article.
- The journal is available online at Wiley Online Library. Visit **www.newphytologist.com** to search the articles and register for table of contents email alerts.
- If you have any questions, do get in touch with Central Office (np-centraloffice@lancaster.ac.uk) or, if it is more convenient, our USA Office (np-usaoffice@lancaster.ac.uk)
- For submission instructions, subscription and all the latest information visit **www.newphytologist.com**